Characterisation of scintillator and gaseous detectors, and Measurement of angular variation of cosmic ray flux with scintillator detector

Project report submitted for the degree of Master of Science

Author:
Shreya Roy

Supervisor:
Dr. Saikat Biswas

Department of Physics
Bose Institute

2017

Dedicated to

My teachers

ACKNOWLEDGMENTS

I gratefully acknowledge the constant and invaluable academic and personal support received from my supervisor Dr. Saikat Biswas. I am really thankful and indebted to him for having been the advisor everyone would like to have, for helping me to learn things in a simpler way and without whose dedicated supervision it would have been never possible to complete this project. I have really enjoyed by working with him.

I would like to thank Dr. Rajarsi Ray, for his interesting discussion and valuable suggestions during the whole M.Sc. course. He has been the substantial sources of inspirations and profound insight during these months.

I have no words to thank Dr. Supriya Das and Dr. Sidharth K. Prasad of Bose Institute for their clear and enthusiastic discussion and valuable suggestions. They have constantly motivated me throughout my study. Without their support it was very difficult to pursue this work.

I am very much indebted to some scientists at Bose Institute especially, Prof. Debapriyo Syam, Prof. Swapan K. Saha, Dr. Sandhya Dey and Dr. Atanu Maulik for their encouragement, support, collaboration and for constantly motivating me in my project work.

I would like to thank Prof. Sanjay K. Ghosh and Prof. Sibaji Raha, for their valuable suggestions and discussions during the course of the study.

I would also like to thank my seniors Mr. Ramaprasad Adak and Mr. Rathijit Biswas for helping me in all possible ways to analyze the results of my experiments. I would also like to thank Mrs. Sharmili Rudra for inspiring, encouraging and helping me in this project.

I am very much thankful to Mr. Dipanjan Nag for helping me to understand the basic electronics and without whom I may not be able to complete this project.

I would like to thank Late Prof. Vladimir Peshekhonov of JINR, Dubna for providing the straw tube prototype and Dr. Subhasis Chattopadhyay, Mr. J. Saini of VECC, Kolkata, Dr. Christian J. Schmidt and Mr. Jörg Hehner of GSI Detector Laboratory for valuable discussions in the course of the study.

I am thankful to Bose Institute workshop for all the mechanical work to build the light guide, coupler. Finally I am thankful to GSI detector laboratory, Germany for providing the optical glue, grease etc. used to build the detector.

I would also like to thank Dr. Subikash Choudhuri of Bose Institute, Mr. Aritra Mondal of Department of Physics, University of Calcutta and Mr. Debdeep Ghosal of Indian School of Mines, Dhanbad, for their help in the study.

I would like to thank Mr. Pratik Ghosal and Mr. Deeptak Biswas for their valuable comments and suggestions during the weekly meeting.

I am also very thankful to my junior Ms. Nilanjana Nandi of Raja Peary Mohan College, University of Calcutta, who worked with me in this project and raised many many questions during the experiment that helped me to learn the subject more clearly.

I would like to acknowledge the support of DST-SERB Ramanujan Fellowship (D.O. No. SR/S2/RJN-02/2012) of Dr. S. Biswas. This work is also partially supported by the research grant of CBM-MUCH project from BI-IFCC, Department of Science and Technology, Govt. of India and the research grant SR/MF/PS-01/2014-BI from Department of Science and Technology, Govt. of India.

Last but not the least I would like to thank my mother, Mrs. Sachi Roy, my uncle Mr. Pravat Singh, my sister Mrs. Sharmistha Roy Nag, My brother in law Mr. Sabyasachi Nag and all relatives for believing in me, for their patience and for their constant support.

Shreya Roy
Kolkata, India

Abstract of The Report

A systematic study of the characteristics of the plastic scintillator detectors has been carried out. Several plastic scintillator paddles and finger are built. The plastic scintillator material and the photomultiplier tube (PMT) are commercially procured. Other components such as Perspex light guide, coupler for light guide are fabricated in proper dimension at Bose Institute workshop. A new and simple technique has been developed using plastic scintillator BC400 detectors for the study of angular variation of cosmic rays at the sea level. The yield uniformity over the entire scintillator area has been checked using Co^{60} and Fe^{55} sources, for a 20 cm $\times$ 20 cm paddle. Efficiency of the paddle detector has also been measured. Detailed detector fabrication process and test results are presented in this report.

As a second part of the project a detailed study of the characteristics of a straw tube detector prototype has been carried out. Straw tube is basically a single wire drift chamber used for particle detection. In this study mainly count rate and ion current produced by the ionising radiation in the detector are measured. The variation of gain and energy resolution of the straw tube detector with voltage has been measured using Fe^{55} spectrum and the results are presented in this report.

Contents

List of Figures

List of Tables

Chapter 1

Introduction

1.1 Detectors: Basic Introduction

The history of radiation detectors parallels the growth in our knowledge of atomic and subatomic physics. An example is Röntgen's discovery of X-rays in 1895 using photographic emulsions. Since that time emulsions have been widely used as radiation detectors. In the following year Becquerel discovered radioactivity with the help of photographic plates. Rutherford used a fluorescent screen and a telescope to view the flashes of light produced by alpha particles on the screen in his famous alpha-scattering experiments. Similar detectors, known as "spinthariscopes", developed by Sir William Crookes in 1903 were the forerunners of the modern scintillation detectors. Electroscopes and electrometers were used to detect the ionization produced by radiations, and these instruments were used in the discovery of cosmic rays. Marie Curie used electrometers in her study of the radioactivity of a wide variety of substances. The extreme difficulty of counting fluorescent flashes prompted Rutherford and Geiger to look for a better detector. The facts that (1) radiations produce ions and (2) ions multiply in a sufficiently high electric field were used by them in the design of their new detectors. In 1908 they announced the perfection of a workable nuclear radiation detector. Since that time, there have been several important advances in methods of detection of nuclear radiation. Experimental studies in various areas of nuclear science and applications of nuclear techniques to other branches of science inevitably involve detection of nuclear radiations and quite often also measurement of their characteristics. The term "nuclear radiations", in general covers a variety of energetic charged and uncharged particles and high energy quanta usually encountered in

studies of atomic and sub-atomic phenomena. The charged particles include electrons, mesons, protons, alpha particles and other energetic atomic ions usually referred to as heavy ions. The neutral radiations include neutrons and electromagnetic radiation such as X-rays, gamma rays and neutrinos [1].

The interaction of radiation with matter is used to detect any radiation. The charged and the uncharged radiations loose energy while traversing matter in different ways. The charged particles interact with matter primarily by Coulomb interaction with the electrons of the medium resulting in excitation and ionization of the atoms and molecules of the medium. The excitation and ionization events are so numerous that the energy loss of the incident particle is very nearly continuous. While the ionization events result in the creation of free charge carriers capable of drifting in an applied electric field, the de-excitation of the excited and ionized atoms results in the emission of luminescence photons. The majority of the nuclear radiation detectors rely on sensing either the free charge carriers or the photons. The classification of detectors are discussed in the next section.

1.2 Classification of Detectors

Detection of radiation is possible because in the interaction of radiation with matter, photons, electron-ion pairs, or electron-hole pairs can be produced. The detectors which depend on the detection of the free charge carriers are usually classified under the general category of ionization based detectors. The detectors sensing the luminescence photons are called scintillation detectors. Table 1.1 lists the different types of detectors currently in use.

1.2.1 Gas Detectors

Gaseous detectors (ionization chambers, proportional counters, and Geiger counters) work because the radiations produce electron-ion pairs in the gas.

Table 1.1: **Nuclear Radiation Detectors**

Name	Type	Primary interaction	Medium
Ionization counter	Signal	Ionization	Gas
Proportional counter	Signal	Ionization	Gas
Geiger counter	Signal	Ionization	Gas
Scintillation counter	Signal	Excitation of electronic levels and associated production of photons	Gas, Liquid and solid
Semiconductor counter	Signal	Production of electrons and holes	Solid
Cloud chamber	Track	Ionization	Gas
Bubble chamber	Track	Ionization	Liquid
Spark chamber	Track	Ionization	Gas and solid

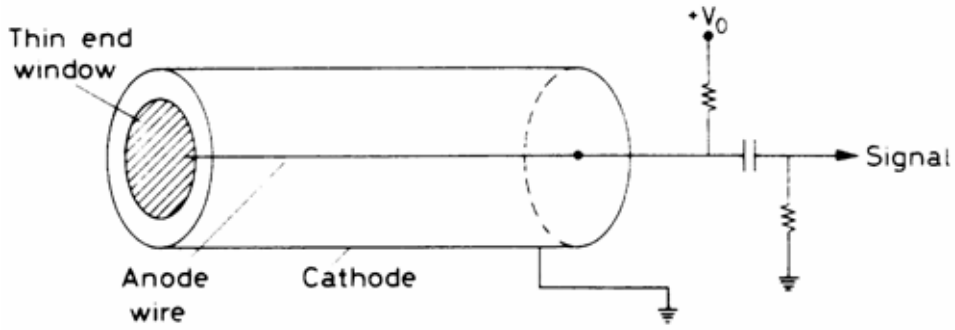

Figure 1.1: Basic configuration of a gaseous detector

The basic configuration of a gas detector consists of a container, lets say a cylinder, with conducting walls (inner side coated with conductor) and a thin end window as shown in Figure 1.1. The cylinder is filled with a suitable gas and a thin conducting wire is suspended along its axis with positive voltage, $+V_0$ relative to the walls. So the cylinder works as a cathode and the central wire works as anode. To understand the working of a gas detector, let us assume (as an example) that radiation of 1 MeV is stopped in the detector. On the average, the incident radiation expends about 30 eV to produce an electron-ion pair, that is, a positive ion and an electron. The number of the primary electron-ion pairs produced by this radiation is,

$$n = 10^6\ eV/30\ eV = 3.3\ \times\ 10^4 \tag{1.1}$$

The mean number of electron-ion pairs created is proportional to the energy deposited in the detector. Since we have electrons and positive ions, their behavior will depend on the electric field inside the chamber. Due to the applied electric field, these electrons will be accelerated towards the anode and the ions towards the cathode where they will be collected. The radial electric field is given by

$$E(r) = \frac{V_0}{r}\frac{1}{ln(\frac{b}{a})} \tag{1.2}$$

where r is the radial distance from the anode, b is the inside radius of the cylinder and a is the radius of the central wire. If there is no electric field or at very low electric field, the ions will recombine with the electrons due to Coulomb attraction. As the applied voltage increases, more and more positive ions and electrons will be collected by the electrodes. The electrons will be collected by the central electrode (which is normally positive) and the positive ions will be collected by the outer electrode. After a certain voltage is reached, all the primary ions, that is, those ions and electrons created directly by the incident radiation, are collected. A plot of the number of ions collected by the electrode versus the applied voltage is shown in Figure 1.2.

In the first region of this figure, called the recombination region, the voltage is insufficient to collect all the ions, which may simply recombine. In the second region, called the ionization region, the electric field is sufficiently large to sweep all the electron-ion pairs to the respective electrodes. A counter operating in this region is called an ionization counter. A further increase in voltage beyond this region shows again an increase in current. At this point, the electric field is strong enough to accelerate freed electrons to energy where they are also capable of ionizing gas molecules in the cylinder. These electrons are known as secondary electrons and they can also be accelerated to produce still more ionizations and so on. As the number of electron-ion pairs in the avalanche is directly proportional to the number of primary electrons, this region is known as Proportional Region. If the voltage is now increased beyond this region, the total amount of ionization created through multiplication becomes sufficiently large that the space charge created distorts the electric field about the anode. This region is known as Limited

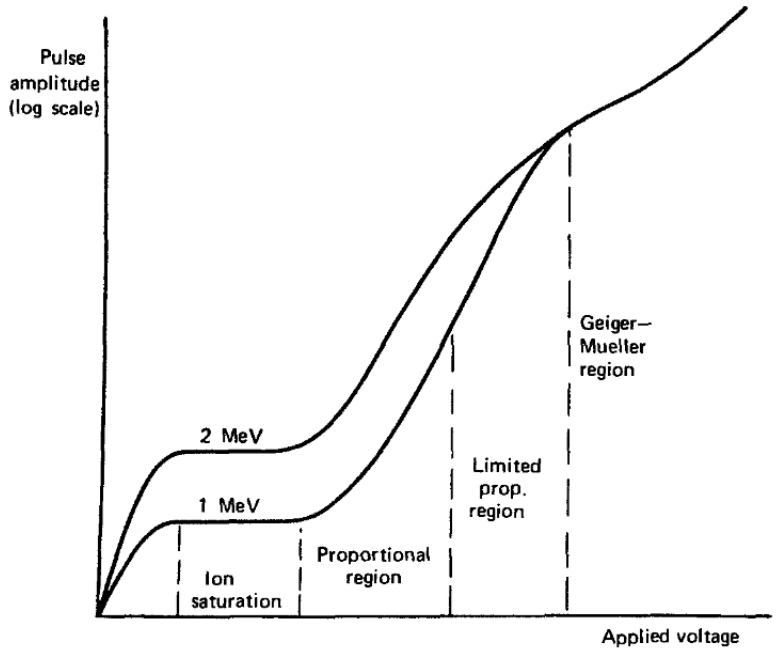

Figure 1.2: The different regions of operation of gaseous detectors.

Proportionality Region. Increasing the voltage still higher, the energy becomes so large that a discharge occurs in the gas. Physically, a chain reaction of many avalanches spread out along the entire length of the anode is triggered by photons emitted by de-excited molecules. The output current thus becomes completely saturated and this region is known as Geiger Muller Region. Further increase in high voltage beyond this region the discharge occurs in the gas. This region is known as Discharge Region.

The electrons travel to the anode with an average velocity known as the drift velocity. This velocity depends on the applied electric field, pressure of the gas, mass of the ion, geometric size of the counter, etc. The drift velocity for the electron is $\sim 10^3$ times the drift velocity of a positive ion. During the transit of the electrons or positive ions, they collide with other ions and atoms in the counter. We can also think of the mean free path for the electrons as the average distance an ion travels between two collisions. With increasing electric field, an electron can gain enough energy in one mean free path to ionize the next atom with which it collides. In this way a multiplication of electrons takes place. The applied potential at which multiplication just starts marks the end of the ionization region and the beginning of a new region called the proportional region. A few examples of detectors operated in proportional

region are, Single Wire Proportional Chamber (SWPC), Multi-Wire Proportional Chamber (MWPC), Gas Electron Multiplier (GEM), Straw-Tube detector.

1.2.2 Scintillator Detectors

In scintillation detectors, radiation-induced excitation produces light quanta (photons). A scintillation counting system consists of a scintillant or scintillator material, a photo-multiplier tube (PMT), a power supply, and an amplifier-analyzer-scaler system. When an ionizing radiation passes through the scintillant, it produces photons. The number of photons produced is proportional to the energy deposited in the scintillator. The scintillator is covered with a reflector except on the side connected to the PMT. The PMT has a photoelectric film (usually coated onto the photomultiplier tube) as its first element. When light falls on it, electrons are released by the photo-electric effect. The number of electrons produced is proportional to the number of photons falling on the photocathode. The electrons produced are focused onto the first dynode. The dynodes are coated with a material like cesium antimonide so that, when high-energy electrons hit them, secondary electrons are produced and hence electron multiplication occurs. The photomultipliers have ten or more dynodes. When an electrical potential is applied between any two dynodes, the secondary electrons produced in preceding dynodes gain energy before they strike the next dynode and produce more secondary electrons. A voltage divider chain is used to provide gradually increasing potential to the dynodes. Finally a large number of electrons are collected at the anode giving a signal.

1.2.3 Semiconductor Detectors

The operation of a semiconductor detector is analogous to the operation of an gas ionization chamber. In an ionization chamber the incident radiation produces positive ions and electrons and an electrical signal is obtained by collecting these ions. In a semiconductor counter the incident radiation produces electrons and holes and information about the radiation is obtained by collecting them. One major difference of course is that only 3.5 eV is needed to produce an electron-hole pair in a semiconductor, while the value is $\sim$30 eV in an gas ionization chamber. The lower energy increases the number of electron-hole pairs per MeV of radiation and decreases the relative statistical variation in this number. Hence the energy resolution is improved and

for this reason semiconductor detectors are used for energy spectroscopy of nuclear physics experiment.

The number of electron-ion pairs, photons, or electron-hole pairs depends on the fraction of the energy of the radiation deposited in the sensitive volume, on the properties of the material, and sometimes on the nature of the radiation. In the design of detectors and in the analysis of information obtained from them, it is important to know how fast the radiations deposited their energy in a medium, how much of it goes into producing electron-ion pairs, photons, or electron-hole pairs, what is the relationship between the number of ions and the energy, and how much material is needed to stop a radiation of a given energy.

1.3 Project Aim/Scope/Objective

There are large number of experimental programs to answer the questions about the origin, composition and structures in the energy spectrum of primary cosmic rays [2, 3, 4, 5, 6, 7]. Various types of particle detection techniques including scintillator detectors of different types, muon tracking chambers have been employed to detect the secondary cosmic ray particles and the particles produced in the air showers.

The main goal of this study is the zenith angle dependence of the cosmic ray flux at the sea level using plastic scintillators. Plastic scintillators are easy to fabricate and operate for cosmic ray muon detection. After the first phase of study with the small size modules we are planning to build large size scintillator detector to detect the muon flux and also the cosmic ray shower at sea level.

The Compressed Baryonic Matter (CBM) experiment at the future Facility for Antiproton and Ion Research (FAIR) in Darmstadt, Germany is designed to explore the QCD phase diagram in the region of moderate baryon densities [8, 9]. This will only be possible with the application of advanced instrumentation, including highly segmented and fast gaseous detectors. Keeping in mind the high interaction rate of FAIR, the Muon Chamber (MuCh) detector in CBM will use Gas Electron Multiplier (GEM) in the first two stations. We are exploring the possibility of straw tubes for the 3^{rd} and 4^{th} stations of CBM-MuCh [10].

Chapter 2

Electronic modules

2.1 Introduction

In this section we will discuss the methods used to extract information from the pulses produced by radiation detectors. A functional or "*blackbox*" approach will be taken to most of the electronic components. The two most common nuclear instrumentation standard are : NIM and CAMAC. The first (and simplest) standard established for nuclear and high energy physics experiments is a modular system called NIM (Nuclear Instrumentation Module). In this system, the basic electronic apparatus, for example, amplifiers, discriminators, etc., are constructed in the form of modules according to standard mechanical and electrical specifications. These modules, in turn, fit into standardized bins which supply the modules with standard power voltages. Any NIM module will fit into any NIM bin [21].

2.2 NIM Bin

The NIM Bin is designed to fit into the standard 19-inch relay rack and is subdivided into 12 individual module positions across its width. A NIM module occupies a unit width of 34.4 mm, although integral multiples of this width are permitted corresponding to modules of double width, triple width, and so on. Each of the 12 bin locations is provided with a 42-pin connector that mates with a corresponding connector at the back of each module. Pin assignments and functions are illustrated in Figure 2.1. Primary dc supply voltages provided by the bin are $\pm$12V

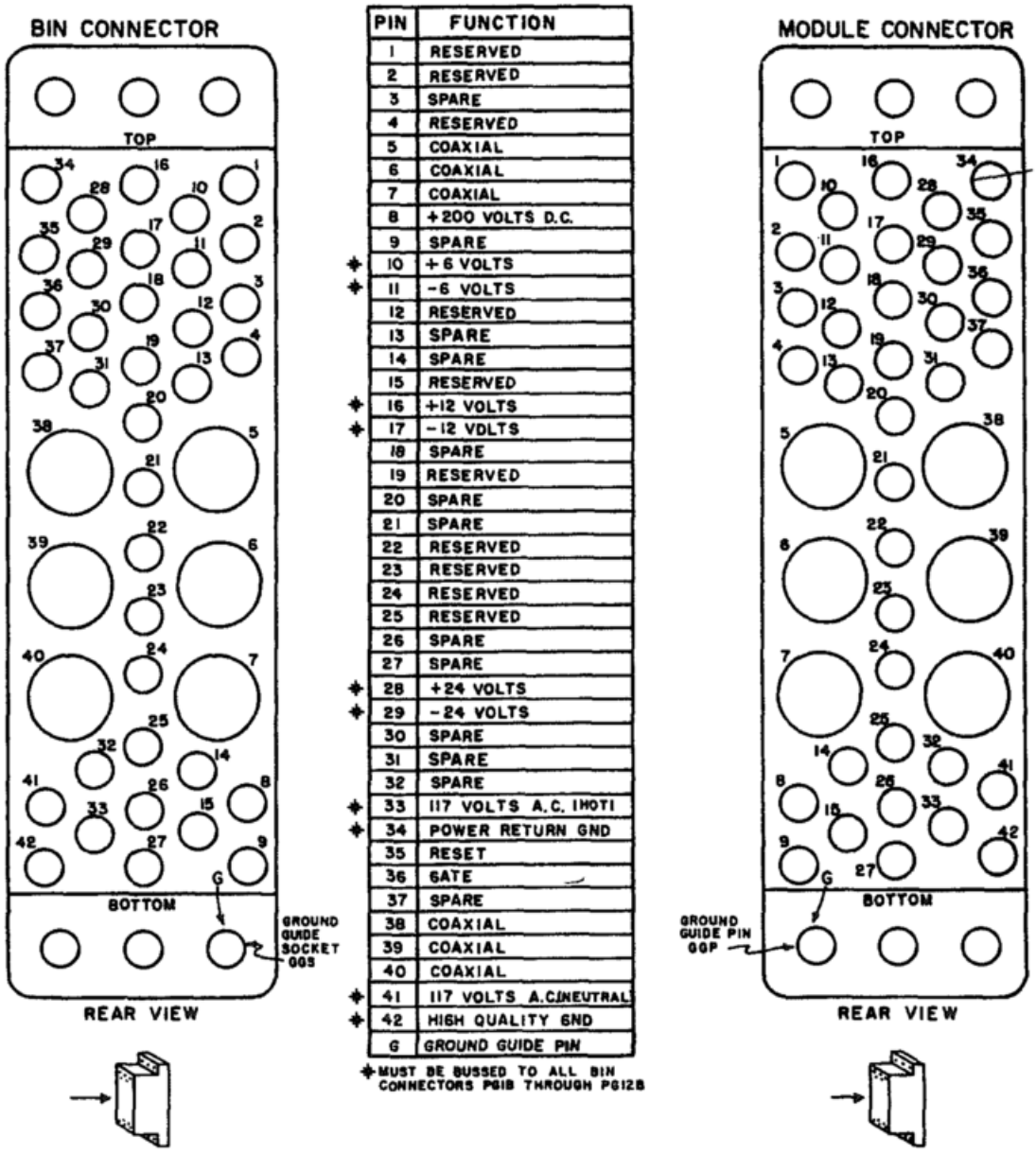

Figure 2.1: Pin assignments for NIM standard connector between bin and module [21].

and ±24V. Some NIM Bins also provide ±6V, mostly for modules using integrated circuits, but these voltages are not strictly required by the NIM rules. The concept of modules in electronic systems offers enormous advantages in flexibility, interchange of instruments, reduced design effort, ease in updating and maintaining the instruments. NIM is the perfect standard for small and flexible setups in the laboratory for high resolution measurements with analogue electronics

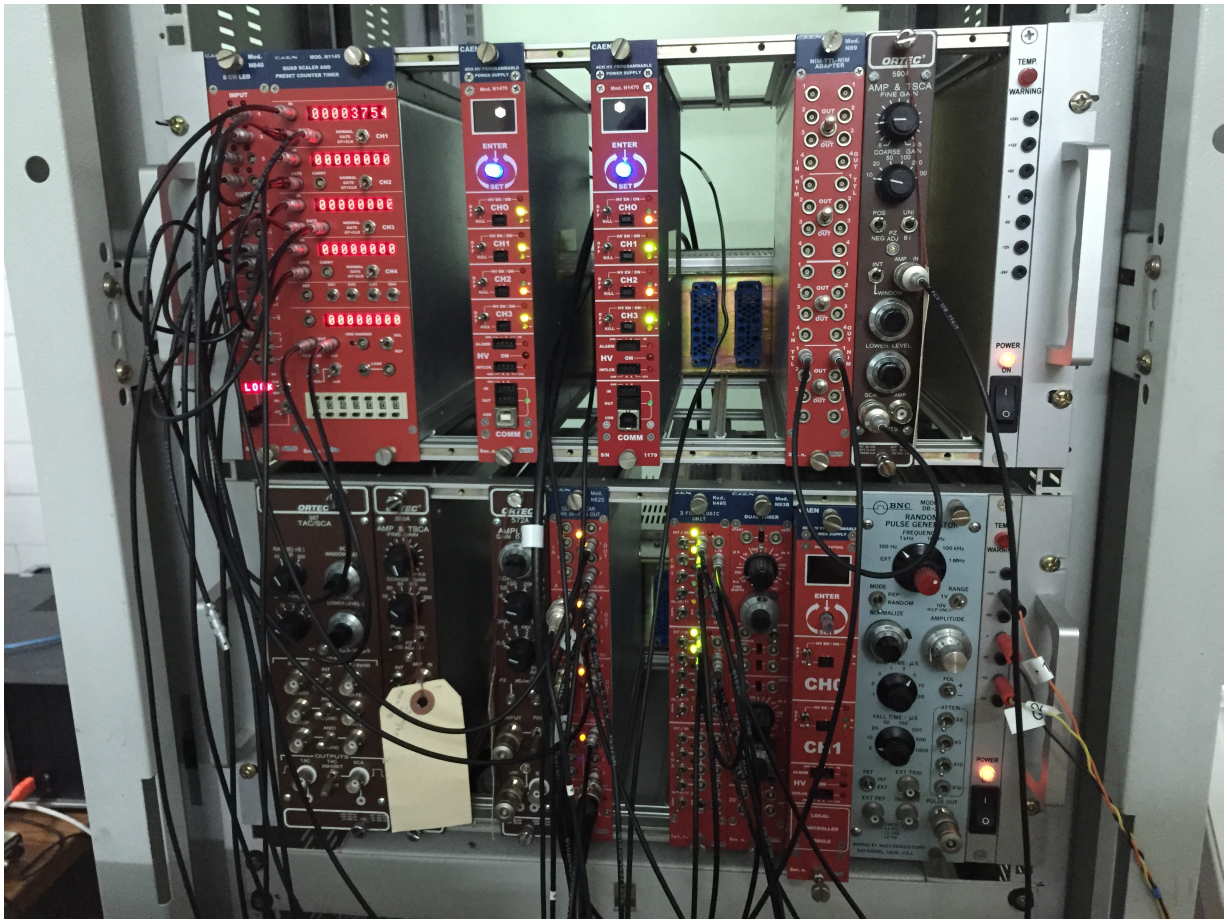

Figure 2.2: NIM Bin with modules.

e.g. amplifier, high resolution analog to digital converter, timing electronics as well as for low or high voltage supplies.

2.3 Basic Modules

The NIM Bin and modules can be of two standard heights: 5.25 inches (133 mm) or 8.75 inches (222 mm), but the larger of these sizes is by far the more common. They can, however, also be built in multiples of this standard, that is, double-width, triple-width [22]. All the NIM electronics modules used in our laboratory are shown in Figure 2.2.

2.3.1 High Voltage Module

High voltage power supply is very important for any detector laboratory. High voltage power supply is used to bias any kind of detector. Sometimes multichannel power supply is necessary for a single detector. It basically consists of a step-up transformer that generates the required high voltage to bias the detector. Different detectors require different biasing voltages in the range of a few hundred volts to a few kV. For example GEM is operated as a voltage $\sim$ 3 - 4 kV, RPC is operated at $\sim$ 8 kV etc. Any desired voltage can be set in the module. The ramp up and ramp down voltages can also be set.

For the plastic scintillator and the straw tube detector testing CAEN 4 channel HV programmable power supply Mod. N1470 has been used. It can supply voltages ranging from 0-8000 Volts.

2.3.2 Preamplifier

The basic function of a preamplifier is to perform impedance matching between the preamplifier input of low capacitance and its output of high capacitance. The preamplifier is not designed to give high gain and usually its gain is of the order of 1-10^2 to amplify weak signals from a detector and to drive it through the cable that connects the preamplifier with the rest of the equipment. At the same time, it must add the least amount of noise possible. Since the input signal at the preamplifier is generally weak, preamplifiers are normally mounted as close as possible to the detector so as to minimize cable length. In this way, pickup of stray electromagnetic fields is reduced and cable capacitance, which decreases the signal-to-noise ratio, minimized.Three basic types of preamplifier exist:

1) voltage sensitive,

2) current sensitive,

3) charge sensitive.

For straw tube detector and GEM detector Ortec 142 IH and VV50-2 preamplifier are used.

2.3.3 FAN IN - FAN OUT (FIFO)

Fan-outs are active circuits which allow the distribution of one signal to several parts of an electronics system by dividing the input signal into several identical signals of the same height and shape. The fan-in, on the other hand, accepts several input signals and delivers the algebraic sum at the output. These modules may be bipolar, i.e., accepting signals of both polarities, or of single polarity, i.e., accepting signals of one polarity only. Fan- ins are particularly useful for summing the outputs of several detectors or the signals from a large detector with many PM's. Both fan-ins and fan-outs come in two varieties: linear and logic. The linear modules accept both analog and logic signals, whereas logic fan-outs and -ins are designed for logic signals only. In the case of a logic fan-in, the algebraic sum is replaced by a logical sum (i.e., OR). In our laboratory CAEN Quad linear FAN IN - FAN OUT Mod. N625 is used.

2.3.4 Discriminator

The discriminator is a device which responds only to input signals with a pulse height greater than a certain threshold value. If this criterion is satisfied, the discriminator responds by issuing a standard logic signal; if not, no response is made as shown in Figure 2.3. The value of the threshold can usually be adjusted by screw on the front panel. As well, an adjustment of the width of the logic signal is usually possible via similar controls. The most common use of the discriminator is for blocking out low amplitude noise pulses from photomultipliers or other detectors. Good pulses, which should in principle be large enough to trigger the discriminator are then transformed into logic pulses for further processing by the following electronics. In this role, the discriminator is essentially a simple analog-to-digital converter. An important aspect of the discriminator is the method of triggering. Because of its use in timing, it is important that the time relation between the arrival of the input pulse and the issuance of the output pulse be constant. In most discriminators, triggering occurs the moment the pulse crosses the threshold level. This is known as leading edge (LE) triggering. For the plastic scintillator testing CAEN 8 CH LED (Mod. N840) has been used.

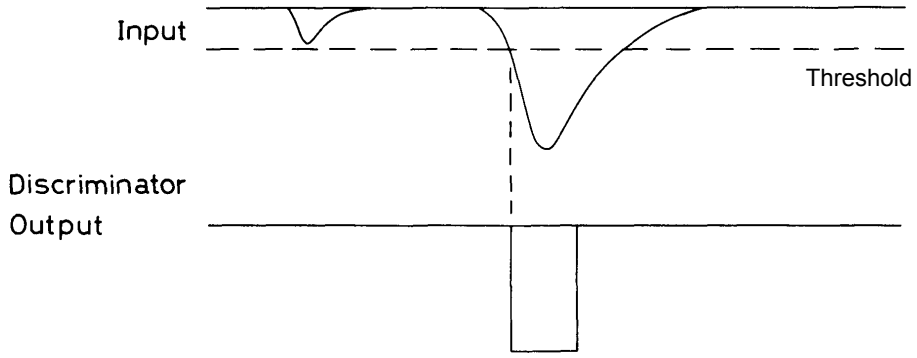

Figure 2.3: Discriminator operation: only signals whose amplitude is greater than the fixed threshold trigger an output signal.

2.3.5 Single channel Analyzers

The single channel analyzer (SCA) or differential discriminator (DD) is a device which sorts incoming analog signals according to their amplitudes. Like the discriminator, it contains a lower level threshold below which signals are blocked. In addition, however, there is also an upper level threshold above which signals are rejected. Thus only signals which fall between these two levels provoke a response from the SCA, i.e., a standard logic signal. This is illustrated in Figure 2.4. The opening between the upper and lower level is usually called the window. With detectors where the output is proportional to energy, the SCA can be used to measure energy spectra by choosing a small, fixed window and systematically sweeping the window across the full pulse height range. The relative number of counts per unit time at each position can then be plotted to give a histogram of the spectrum. The SCA generally has three working modes:

1) Normal Mode or Differential Mode - In this mode, the upper (ULD) and lower (LLD) levels can be adjusted independently of each other, that is the settings of the LLD has no effect on the setting of the ULD and vice-versa.

2) Window Mode - In this mode one sets the lower level and the window width, that is the distance between lower and upper levels.

3) Integral Mode - Here, the upper level is completely removed from the SCA circuit altogether so that one simply has a discriminator with an adjustable lower level.

In this study Ortec 590A AMP & TSCA module is used.

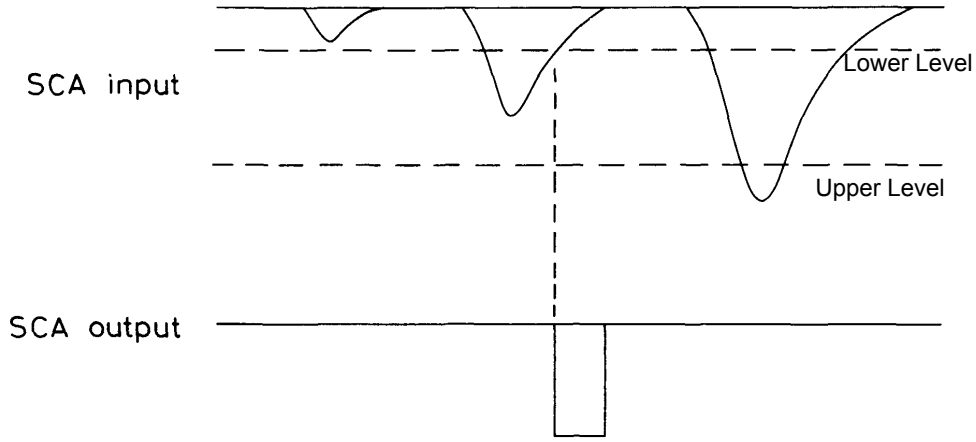

Figure 2.4: Basic operation of a SCA: only signals whose amplitude fall within the window defined by the upper and lower level threshold trigger an output signal.

2.3.6 Multichannel Analyzers

Multichannel analyzers (MCA) are sophisticated devices which sort out incoming pulses according to pulse height and keep count of the number at each height in a multichannel memory. The contents of each channel can then be displayed on a screen or printed out to give a pulse height spectrum. The MCA works by digitizing the amplitude of the incoming pulse with an analog-to-digital converter (ADC). The MCA then takes this number and increments a memory channel whose address is proportional to the digitized value. In this way incoming pulses are sorted out according to pulse height and the number at each pulse height stored in memory locations corresponding to these amplitudes. The total number of channels into which the voltage range is digitized is known as the conversion gain. This determines the resolution of the MCA. Conversion gains of 128 up to 8 K or 16 K are often found on commercial MCA's.

2.3.7 Coincidence Units

The coincidence unit determines if two or more logic signals are coincident in time and generates a logic signal if true and no signal if false. The electronic determination of a coincidence between two pulses may be made in a number of ways. One method is to use a transmission gate as we have seen. Another simple method often used is to sum the two input pulses and to pass the summed pulse through a discriminator set at a height just below the sum of two logic pulses.

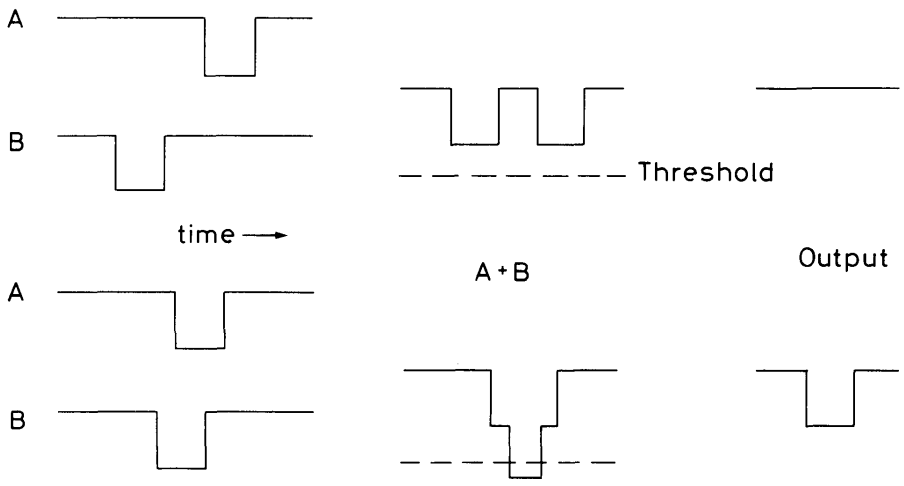

Figure 2.5: The summing method for determining the coincidence of two signals. The pulses are first summed and then through a discriminator set at a level just below twice the logic signal amplitude.

This method is shown in Figure 2.5. Obviously, the sum pulse will only be great enough to trigger the discriminator when the input pulses are sufficiently close in time to overlap. The definition of coincidence, here, actually means coincidence within a time such that the pulses overlap. This time period determines the resolving time of the coincidence and depends on the widths of the signals and the minimum overlap required by the electronics. In this study CAEN Mod. N405 3 fold logic unit is used.

2.3.8 Cathode Ray Oscilloscope

To visualize the signal produced by the detector and study various characteristics of the pulse, such as rise time, fall time, pulse height, pulse shape, etc. Cathode Ray oscilloscope (CRO) is used. In the CRO one can set trigger and threshold to encounter only useful events and to cut off the noise respectively. The CRO used in this experiment is from Agilent Technologies and can support up to four different input signal ports.

2.3.9 Scaler / Counter

The scaler is a unit which counts the number of pulses fed into its input and presents this information on a visual display. In general, scalers require a properly shaped signal in order to function correctly; thus it is usually necessary to have a discriminator or a pulse shaper process signals from the detector before they can be counted by the scaler. Most commercial scalers are also available with a variety of auxiliary functions such as a gate, preset count, reset, etc. Scaler can accept NIM or TTL signals as input. In this study CAEN Mod. N1145 Quad scaler and preset counter timer is used.

2.4 NIM Logic Signals

NIM modules include both analog and digital instruments. It should be recalled that in analog signals, information is carried in the amplitude or shape of the signal, thus they are of continuously varying heights and form. Digital or logic signals, on the other hand, are of fixed shape and have only two possible states: yes or no. It is customary to refer to the two states as logical 0 and logical 1; which signal is chosen as 1 or 0 is arbitrary however. Two types of standards exist: slow-positive logic and fast-negative logic. The first refers to signals of relatively slow rise time, on the order of hundreds of nanoseconds or more. They are of positive polarity and are used with slow detector systems. Table 2.1 defines the voltage levels for this logic. Note that the definition is in terms of a voltage across a 1000 Ω impedance. This implies that the current carried by the signal is very small. The consequence of this is that slow-positive signals cannot be transmitted through long cables. The characteristic impedance of most cables is not more than about 100 Ω. After a meter or two of cable, therefore, the signal becomes highly attenuated.

Fast-negative logic, often referred to as NIM logic, employs extremely fast signals with rise times on the order of 1 ns and comparable widths. This type is often used in experiments using fast plastic counters (in high-energy physics, for example) where high count rates or fast timing is desired. The NIM logic levels are defined in Table 2.1 . Note that unlike slow-positive logic, the definition is current based rather than voltage based.

Table 2.1: **NIM Logic Standards**

Type	Logic	O/P must deliver	I/P must accept
Fast negative	Logic 1	-14 mA to -18 mA	-12 mA to -36 mA
	Logic 0	-1 mA to +1 mA	-4 mA to +20 mA
Slow positive	Logic 1	+4 V to +12 V	+3 V to +12 V
	Logic 0	+1 to -2 V	+1.5 V to -2 V

2.5 TTL AND ECL

While not part of the NIM standard two other logic families are often found in nuclear and particle physics electronics. The first is the TTL (Transistor-Transistor Logic) logic family. This is a positive going logic which is very often found on NIM electronics modules. The levels are defined in Table 2.2. The second is a logic family which is becoming increasingly popular in high-energy physics. This is the emitter-coupled logic (ECL) family which is currently the fastest form of digital logic available. These levels are also defined in Table 2.2.

Table 2.2: **TTL and ECL signal levels**

Logic	TTL	ECL
Logic 1	2-5 V	-1.75
Logic 0	0-0.80 V	-0.90 V

Chapter 3

Study of some aspects of straw tube detectors

3.1 Introduction

Basic R & D have been carried out with one straw tube detector prototype with premixed gas of Ar+CO_2 70:30. The count rates are measured with Fe^{55} radioactive source. The attenuation of signal and the uniformity of performance are also measured. The gain and energy resolution are measured from Fe^{55} The details of the measurement process and the experimental results are presented in this report.

In our laboratory R & D are being carried out on several gas filled and scintillator detectors. The program includes R & D on Gas Electron Multiplier (GEM) detectors [11], plastic and NaI scintillator detectors. Very recently we have started to study the characteristics of straw tube detectors with conventional Argon based gas mixture. Straw tubes are currently being used in large High Energy Physics (HEP) experiments as tracking detector with low material budget [12].

The Compressed Baryonic Matter (CBM) experiment at the future Facility for Antiproton and Ion Research (FAIR) in Darmstadt, Germany is designed to explore the QCD phase diagram in the region of moderate baryon densities [8, 9]. This will only be possible with the application of advanced instrumentation, including highly segmented and fast gaseous detectors. Keeping in mind the high interaction rate of FAIR, the Muon Chamber (MuCh) detector in CBM will

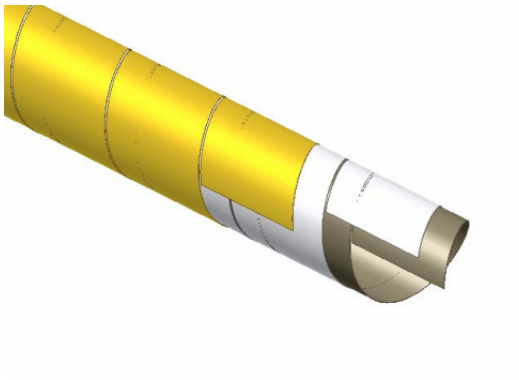

Figure 3.1: The straw tube [taken from TDR CBM MuCh Report]

use Gas Electron Multiplier (GEM) in the first two stations. We are exploring the possibility of straw tubes for the 3^{rd} and 4^{th} stations of CBM-MuCh [10].

3.2 The Straw tube detector

The straw tube detector is a single wire gas detector. It has two basic components, namely the straw (cathode) and the anode wire.

3.2.1 The straw

The structure of a straw tube is shown in Figure 3.1 Straw tube is typically prepared from a kapton film, one side containing a conductive layer of 1000-3000 $\mathring{A}$ Al + 4 μm carbon-loaded kapton and the other side containing a thermoplastic polyurethane layer of 3 μm [13]. The inner surface of the straw is used as cathode. The straws are manufactured by industrial method. The first step is the preparation of the film, second one is the preparation of the film strips with the width of 8$\pm$0.1 mm. Two kapton film tapes (4-8 mm wide) are wound in spiral at a temperature around 200 ^{o}C. The thickness of the straw wall is around 60 μm.

3.2.2 Anode wire

The anode for the straws is a gold-plated tungsten (with 2% of rhenium) wire with a 30±0.3 micron diameter (type 861, Luma). The anode wires are centered in the straws by two end-plugs and four small plastic spacers. The electrical resistance of this wire is about 60 Ω/m. The wire tension will be set to 70±10 g, close to the elastic limit which is around 1.2 N. The wire should meet following requirements.

- Wire ellipticity should correspond to wire diameter variation of ±2%.
- The base wire must be free of defects, specifically cracks, splits etc.
- Base wire should be electrically polished to provide a smooth surface free from any defects.
- The base wire surface should be also carefully treated (light electrolytic cleaning) to eliminate all traces of oxides and other possible pollutants just before gold plating.
- The base wire is to be plated with pure gold. No nickel additives to the gold, no Ni-flashing of the wire surface before gold plating are allowed.
- The finished, gold plated wire must have a clean surface which is free of any contaminant, e.g. oil, dirt, dust, fibres, chemical residuals etc. No mechanical treatment of the wire surface is allowed after gold plating.

The wire is intended to be used without further cleaning at the production sites. The straw cathode will be grounded and the anode will be under high voltage.

3.3 Working principle of straw tube

A straw tube detector is basically a gas filled single channel drift tube with a conductive inner layer as cathode and a wire stretched along the cylindrical axis as anode. When high voltage is applied between the wire and the tube an electric field is generated in the gas filled region. The electric field separates electrons and positive ions produced by an incident charged particle

along its trajectory through the gas volume. The wire is kept at positive voltage and collects the electrons while the ions drift towards the cathode. By choosing thin wires, with a diameter of a few tens of μm, the electric field strength near the wire is made high enough to create an avalanche of electrons. Depending on the high voltage and the gas composition a gain of about 10^4 - 10^5 can be achieved [14]. The specific energy loss (dE/dx) of a charged particle in the straw gas volume can be used to identify the particle species and can be derived from the number of ionization electrons per track length (dx) for the generated straw signal. Main idea of using straw tube in a tracking system is reduction of material budget.

3.4 Choice of fill gas

The choice of a filling gas for proportional counters is governed by several factors like low working voltage, high gain, good proportionality and high rate capability. In general, these conditions are met by using a gas mixture rather than a pure one. For a minimum working voltage, noble gases are usually chosen since they require the lowest electric field intensities for avalanche formation and also they do not undergo chemical reactions with the material of the detector. Argon is usually preferred because of its higher specific ionization and lower cost. Pure argon as a filling gas, however, cannot be operated with gains of more than about $10^3 - 10^4$ without continuous discharge occurring. This arises because of the high excitation energy (11.6 eV) for this element. Excited argon atoms formed in the avalanche thus de-excite giving rise to high energy photons capable of ionizing the cathode and causing further avalanches. This problem can be remedied by the addition of a polyatomic gas, such as methane or alcohol. A few inorganic gases, such as CO_2, BF_3 can also be used. These molecules act as quenchers by absorbing the radiated photons and then dissipating this energy through dissociation or elastic collisions that is non-radiative. A small amount of polyatomic gas already produces dramatic changes in counter operation. Indeed gains of up to 10^6 are obtained. Another often used quencher is isobutane. In our experiment, the gas used to fill the straw tube detector is 70% Argon and 30% CO_2.

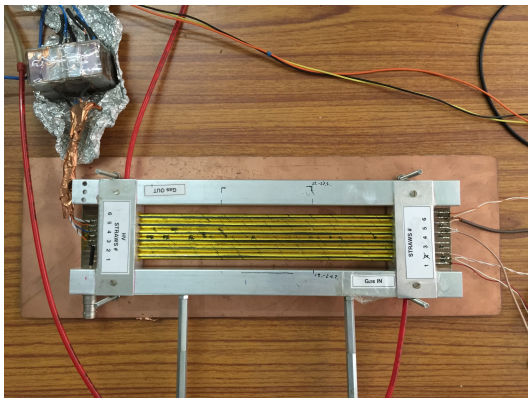

Figure 3.2: The straw tube prototype : 6 straws, each of diameter 6 mm and length 20 cm

3.5 Experimental set up

A straw tube prototype shown in Figure 3.2 is obtained from JINR, Dubna, Russia with 6 straws of diameter 6 mm and length 20 cm. A premixed gas of Argon and CO_2 in 70/30 volume ratio is used in flow mode at a rate of 3 lt/h. The detector is tested using conventional NIM electronics. The positive high voltage (HV) is applied to one end of the central wire of the straws using a HV filter box and the signal is collected from the other end through a capacitor using LEMO connector. Single HV channel is used for each straw tube. A typical Fe^{55} signal in the oscilloscope at 1650 V is shown in Figure 3.3 with settings 20 mV/Div, 20

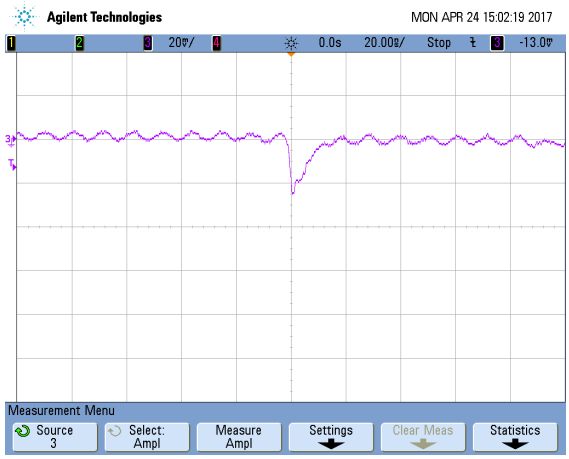

Figure 3.3: The Fe^{55} signal in the oscilloscope at 1650 V (20 mV/Div, 20 ns/Div, 50Ω load)

ns/Div, 50 Ω load. The output signal from the straw is fed to a pre-amplifier and the output of the pre-amplifier is put to a timing SCA (Single Channel Analyzer).

The SCA is operated in integral mode and the lower level in the SCA is used as the threshold to the signal. The discriminated TTL signal is fed to a TTL-NIM adopter and the output is counted using a NIM scaler. The count rate (i.e. counts per second) of the detector is then calculated.

The current due to ions collected at the cathode is measured from the HV power supply.

3.6 Results

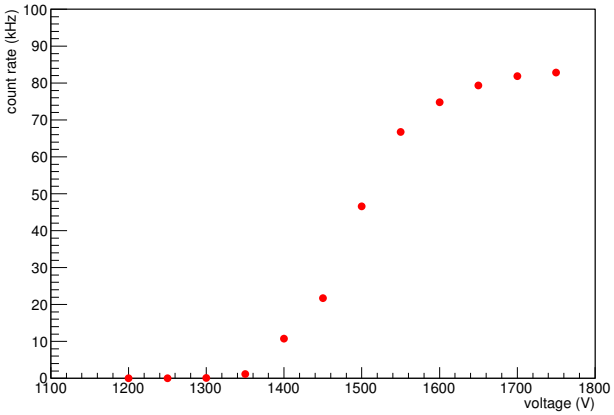

Figure 3.4: The counting rate as a function of applied HV for Fe^{55} source (Threshold to the SCA : 1 Volt).

In this measurement counts from the detector and the ion current are measured. The count rate is measured varying the threshold at a constant HV of 1700 V and it is found that the threshold of 1 V at the SCA is enough to cut all the noise. For the voltage scan, the source with a collimator is kept on the straw and the count is measured with and without the Fe^{55} source varying the HV from 1100 V to 1750 V. The count rate is then calculated for the source only. The variation of count rate as a function of voltage is shown in Figure 3.4. A plateau in the count rate is observed around 1600V and above [15].

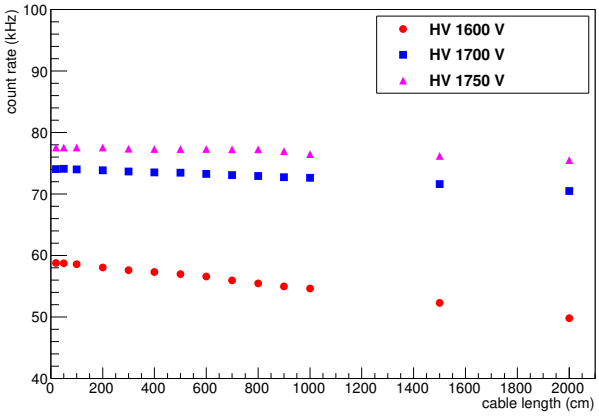

Figure 3.5: The counting rate as a function of cable length.

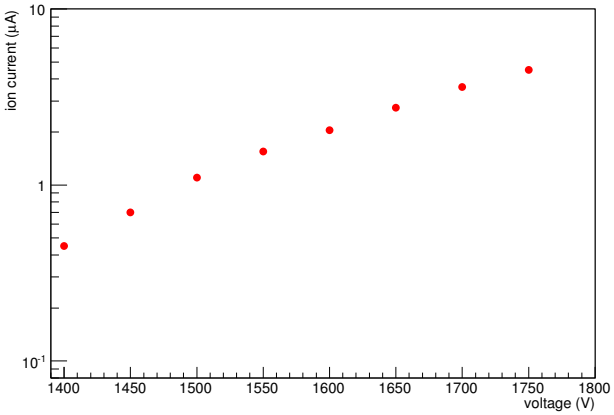

Figure 3.6: Ion current as a function of voltage.

Measurements of signal attenuation by extending the length of the cable, between the pre-amplifier output and the SCA, is carried out. The LEMO cable length is gradually increased from 20 cm to 20 m and the count rates are measured. This measurement is repeated for three biasing voltages 1600 V, 1700 V and 1750 V respectively. The count rate as a function of cable length is shown in Figure 3.5. It is observed that though at lower voltage the count rate is decreasing with increasing cable length the effect decreases at higher voltages.

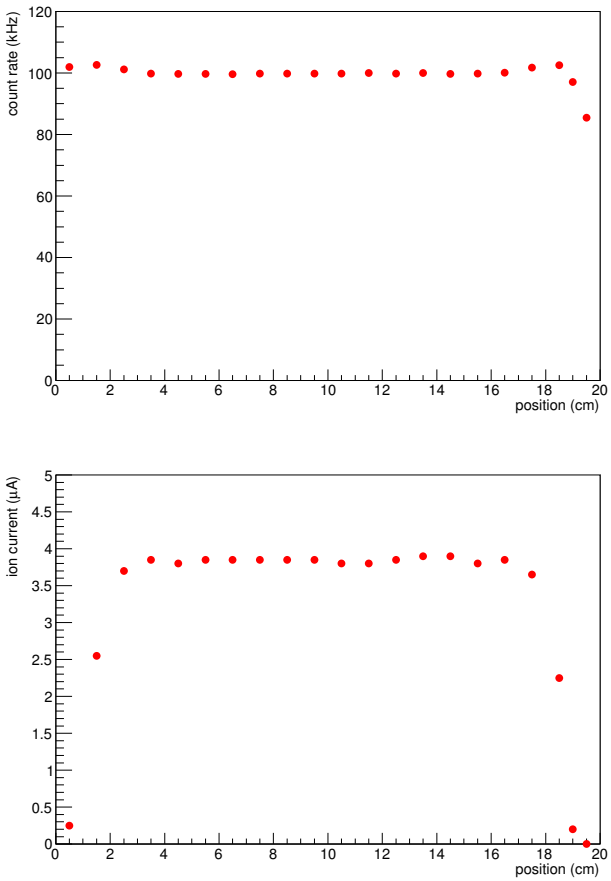

Figure 3.7: (Top) Uniformity of count rate along the length. (Bottom) Uniformity of ion current along the length.

The ion current or the relative gain of the straw has been studied. The ion current is measured from the HV power supply. The variation of the ion current as a function of voltage is shown in Figure 3.6.

The uniformity of count rate and the ion current along the length of the straw has been checked by placing Fe^{55} source at different positions on the length of the straw. The HV to the straw is set at 1750 V and count rate and ion currents are measured. The uniformity of rate and ion current are shown in Figure 3.7. Both the rate and ion current are uniform over the length of the straws except at the edges.

The energy spectrum of the straw tube detector is obtained for Fe^{55} X-ray source using an MCA. Figure 3.8 shows a typical spectrum recorded with a straw tube detector for Fe^{55} source

at a biasing voltage of 1625 V. In the spectrum the main peak (5.9 keV full energy peak) and the escape peak are visible and well separated from the noise peak.

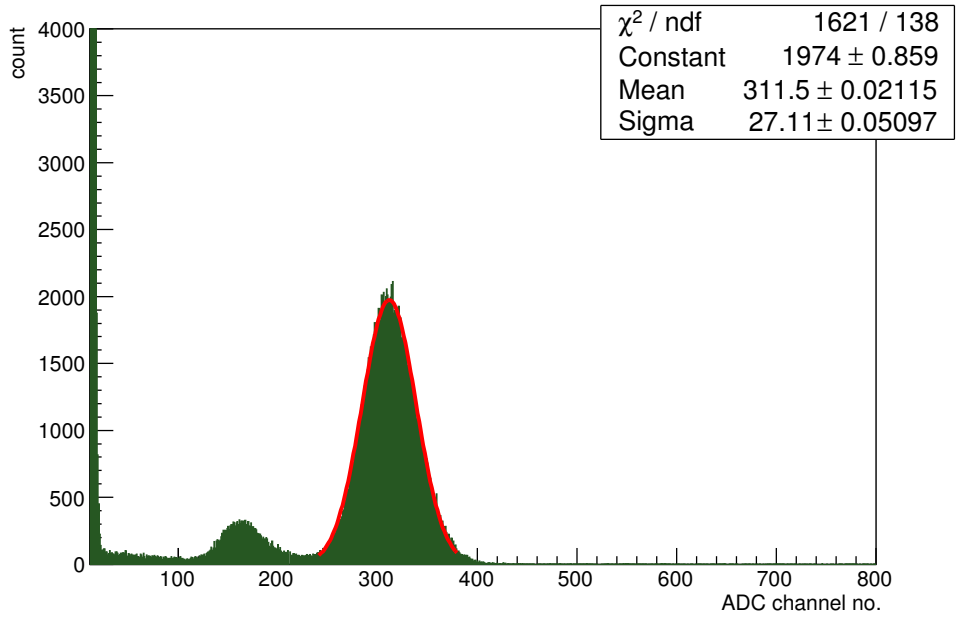

Figure 3.8: Energy Spectrum of the Straw Tube Detector.

The gain and energy resolution of the Straw Tube detector has also been measured. The gain of the detector has been measured by obtaining the mean position of 5.9 keV peak of Fe^{55} X-ray spectrum with Gaussian fitting.

The expression for gain is given by:

$$gain = \frac{output\ charge}{input\ charge} \tag{3.1}$$

$$= \frac{(mean\ pulse\ height\ for\ 5.9\ keV\ peak/2mV)fC}{212\ \times\ e\ C} \tag{3.2}$$

where the mean pulse height for 5.9 keV peak in ADC channel number is obtained by gaussian fitting and that in mV is obtained from the ADC calibration curve (pulse height vs ADC channel no.). The preamplifier offers a gain of 2 mV/fC which has been used in the expression for gain. The input charge is the primary number of electrons produced in the gas detector as a result of total absorption of an X-ray photon of energy 5.9 keV. For Ar-CO_2 gas in the ratio 70:30 the number of primary electrons produced is 212 approximately.

The energy resolution of the detector is defined as:

$$\%\ energy\ resolution = \frac{sigma\ \times\ 2.355}{mean}\% \tag{3.3}$$

where the sigma and the mean are obtained from the gaussian fitting of the spectrum. It is understood that a lower value of energy resolution means a better energy resolution. The gain and energy resolution has been calculated increasing the biasing voltage of the Straw Tube detector. It is observed that the gain increases exponentially and the energy resolution value decreases with the voltage as shown in Figure 3.9.

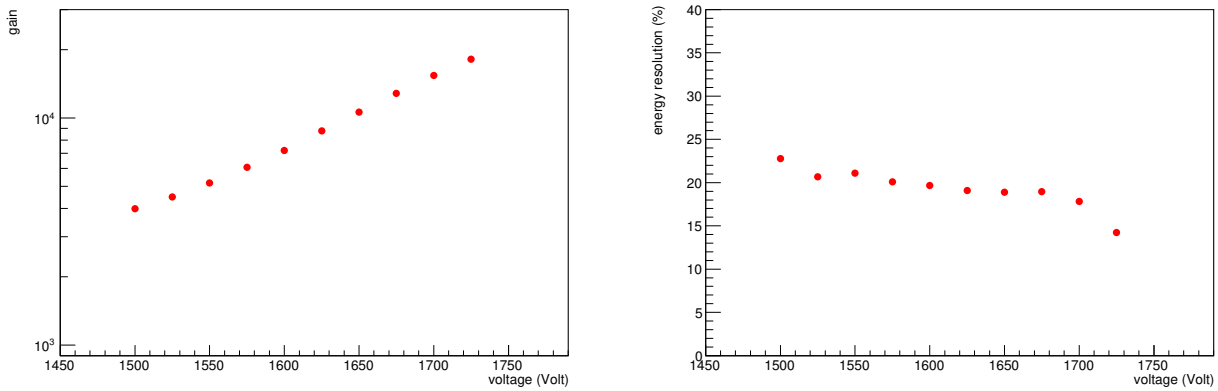

Figure 3.9: Gain (left) and energy resolution (right) as a function of voltage.

3.7 Summary and outlooks

Basic characteristic studies are performed for straw tube detector with Ar+CO_2 gas in 70:30 ratio using conventional NIM electronics. In this study count rate, ion current or the relative gain, signal attenuation and uniformity of performance are studied systematically. The energy spectrum is also obtained using MCA. The gain and energy resolution are measured. Use of the straw tube detector in CBM MuCh is under investigation.

Chapter 4

Characterization of plastic scintillator detector

4.1 Introduction

Scintillators are materials that are able to convert energy deposited by high energy charged particles like muons, pions etc. into photons of near visible region. They are of gaseous, liquid or solid materials and either organic or inorganic. The requirements that a scintillator detector should have are:
1) High efficiency for conversion of exciting energy to fluorescent radiation.
2) Transparency to its fluorescent radiation.
3) Emission in a spectral range consistent with the spectral response of existing photomultipliers.
4) Short decay constant.

A systematic study of the characteristics of the plastic scintillator paddle detector has been carried out. The yield uniformity of the detector is also measured. The details of the measurement and the experimental result are presented in this report. The motivation of this work is to measure the cosmic ray flux at different zenith angles at the sea level, using plastic scintillation detector.

Two scintillator detector modules using BC400 plastic have been fabricated and tested with cosmic ray muons and different radioactive sources. As a proof of principle a preliminary study

has been carried out using one paddle scintillator (named Sc-01) of dimension 20 cm $\times$ 20 cm and one finger scintillator (named Sc-02) of dimension 10 cm $\times$ 2 cm, each of thickness 1 cm, to measure the angular variation of cosmic ray flux [16, 17, 18, 19]. The plastic scintillator material and the photomultiplier tube (PMT) are commercially procured. All other components such as Perspex light guide, coupler for light guide are fabricated in proper dimension at Bose Institute workshop. In this experiment the conventional NIM electronics is used. The data analysis is carried out using ROOT software package [20].

In this report the details of building of the scintillator detectors are given in Sec 4.2, the experimental set-up is described in Sec 4.3, the measurement technique and results are shown in Sec 4.4.

4.1.1 Plastic Scintillator

Plastic scintillator is one of the important detectors to detect particle produced in high-energy physics experiment. It is the device with scintillating material coupled with an amplifier to convert scintillation light into electrical signal and can be counted or analyzed. It offers an extremely fast signal. The main advantage of these detectors is their flexibility. They can be made of any size. The main purpose of our R&D of this kind of scintillator is to study the physics of cosmic ray and also to use it as trigger for gaseous detectors.

Plastic scintillators have relatively short response time. Typically of the order of few nano seconds. Plastic scintillators are reliable, robust, and convenient. However, they possess quirks to which the experimenter must be alert. Exposure to solvent vapours, high temperatures, mechanical flexing, irradiation, or rough handling will adverse the processes. A particularly fragile region is the surface which can develop micro-cracks which degrade its transmission of light by total internal reflection. A charged particle traversing these plastic material leaves behind some excited molecules. Certain types of molecules, however, will release a small fraction (about 3%) of this energy as optical photons. This process, scintillation, is especially marked in those organic substances which contain aromatic rings, such as polystyrene (PS) and polyvinyltoluene (PVT). The scintillator material used in this experiment has polyvinyltoluene (PVT) as its base and contains 65% anthracene. A scintillator detector has three main components:

1) Scintillator material

2) Light guide

3) Photomultiplier tube shown in Figure 4.1

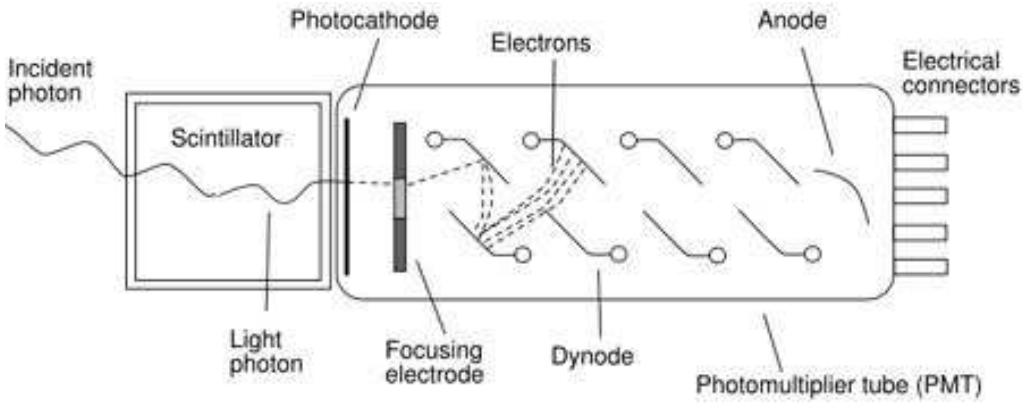

Figure 4.1: Main Parts of the plastic scintillator

4.1.2 Photomultiplier tube

Photomultipliers (PM's) are devices which convert light into a measurable electric current. They are extremely sensitive and mostly used in nuclear and high-energy physics experiments. Figure 4.1 shows a schematic diagram of a typical photomultiplier. It consists of a cathode made of photosensitive material followed by an electron collection system, an electron multiplier section (or dynode string as it is usually called) and finally an anode from which the final signal can be taken. All parts are usually housed in an evacuated glass tube. During operation a high voltage is applied to the cathode, dynodes and anode such that a potential "ladder" is set up along the length of the cathode - dynode - anode structure. When an incident photon (from a scintillator for example) impinges upon the photocathode, an electron is emitted via the photoelectric effect. Because of the applied voltage, the electron is then directed and accelerated toward the first dynode, where upon striking, it transfers some of its energy to the electrons in the dynode. This causes secondary electrons to be emitted, which in turn, are accelerated towards the next dynode where more electrons are released and further accelerated. An electron cascade down the dynode string is thus created. At the anode, this cascade is collected to give a current which can be amplified and analyzed.

4.2 Building of the scintillator modules

One BC400 type 40 cm × 40 cm scintillator plate of thickness 1 cm is procured. At Bose Institute workshop this plate is cut into several small pieces to build scintillator detectors.

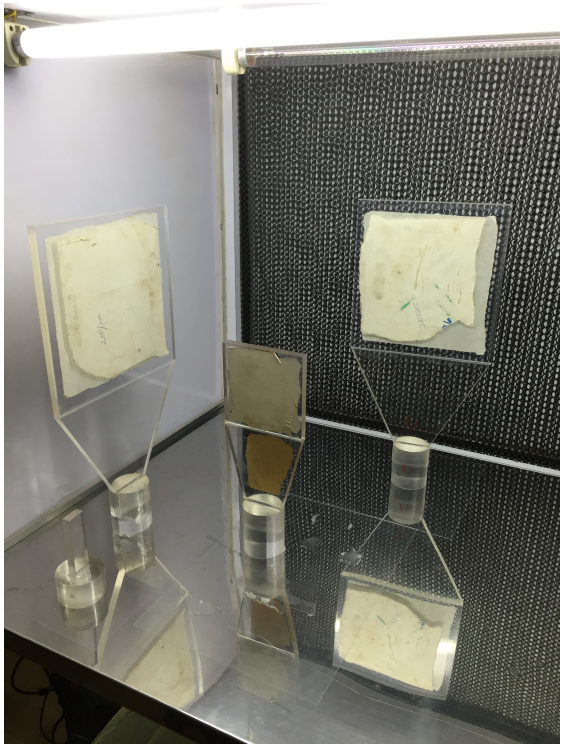

Figure 4.2: Gluing of scintillator with the light guide

Figure 4.3: Wrapping with Tyvek paper (left) and with black tape (right)

For this particular study the plastic scintillator paddle detector has dimension 20 cm × 20 cm. Whereas the finger scintillator detector is of size 10 cm × 2 cm. For the scintillator paddle the

Figure 4.4: Application of optical grease to PMT

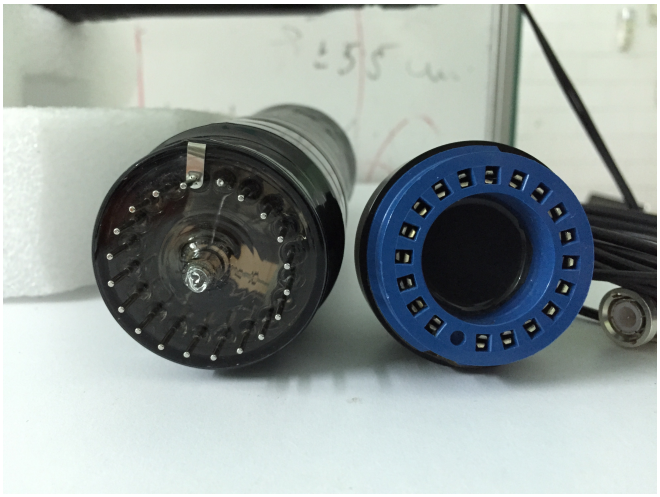

Figure 4.5: PMT and base of voltage divider

Perspex light guide is trapezoidal in shape whose longer side (connected to scintillator) is 20 cm, shorter side (connected to one side of the cylindrical light guide) is 5.1 cm and length about 15 cm. The cylindrical light guide other side which is connected to the PMT has diameter 5.1 cm.

The plastic scintillator BC400 has been glued with the light guide with BC-600 optical cement and hardener in the ratio 5 : 1, which is a clear epoxy resin that sets at room temperature and has a refractive index close to that of our premium plastic scintillators. After gluing the different components, the scintillator modules have been left for curing for 24 hours at room

Figure 4.6: Completed scintillator paddle detector

temperature as shown in Figure 4.2. After that the entire thing has been wrapped tightly with Tyvek paper using paper tapes. Then black tapes have been wrapped around the scintillator as shown in Figure 4.3. The PMT has been joined to the cylindrical light guide using optical grease as shown in Figure 4.4. The entire assembly of scintillator and PMT has been wrapped with black tapes twice to ensure no light leakage. Then the base voltage divider circuit is connected to the PMT. In the base there is one SHV cable with connector for the application of high voltage and one BNC cable with connector for the signal. The base voltage divider circuit and the pins of the PMT are shown in Figure 4.5. The complete scintillator paddle detector is shown in Figure 4.6. In total two paddle detector of dimension 20 cm $\times$ 20 cm, one paddle of dimension 10 cm $\times$ 10 cm and one finger of 10 cm $\times$ 2 cm have been built.

4.3 Experimental Set-up

All the scintillator detectors are placed in a specialized aluminium rack where both vertical (y axis) and horizontal (x axis) movements are easily possible.

At first the operating voltage and threshold for the discriminator are optimized for all the modules. The bias voltages to the PMT are gradually increased and the count rate are measured for cosmic ray and also for different radioactive sources. A schematic circuit arrangement of the scintillator detector and electronics for the singles count from a scintillator module is shown in

Figure 4.7. The discriminated NIM signals are put to a logic unit and the coincidence count has been measured using a NIM scaler.

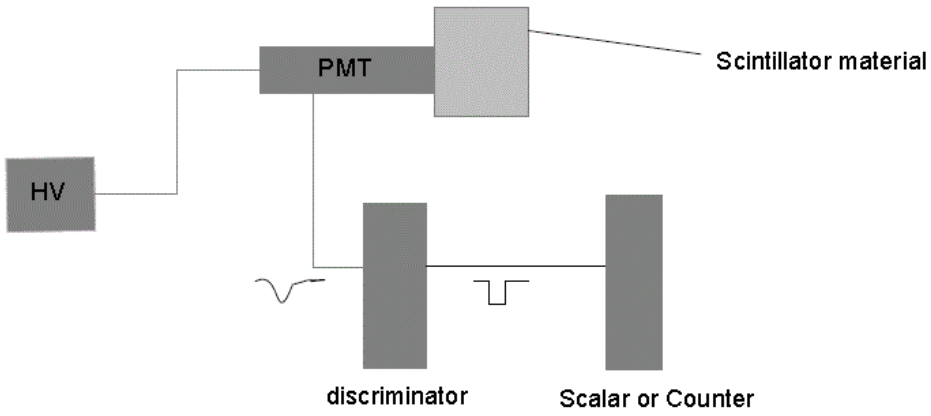

Figure 4.7: Complete circuit arrangement for a scintillator detector

The efficiency of a scintillator detector is measured with cosmic ray by triggering with other scintillator detector. In this chapter basic characterization of the scintillator modules are described.

4.4 Measurements and results

The counts from each scintillator detector is measured for different radioactive sources and cosmic rays, varying the applied high voltage to the PMT and threshold to the discriminator to get its operating point (operating voltage and threshold).

4.4.1 Calibration of the Photomultiplier Tube

The PMT has been calibrated by measuring the count rate of the scintillator paddle and the finger varying the applied voltages to the PMT from 1000 V to 1850 V. The thresholds have been set at -50 mV to the Leading Edge Discriminator (LED). For each voltage settings count rates have been measured using three different radioactive sources e.g. Cs^{137}, Na^{22}, Co^{60}. The cosmic ray background count has also been taken for each settings and it is subtracted from

the count taken with source. It is observed that for each sources the count rate increases with voltage and reaches a plateau for voltage $\sim$ 1600 V and onwards. The results are shown in Figure 4.8.

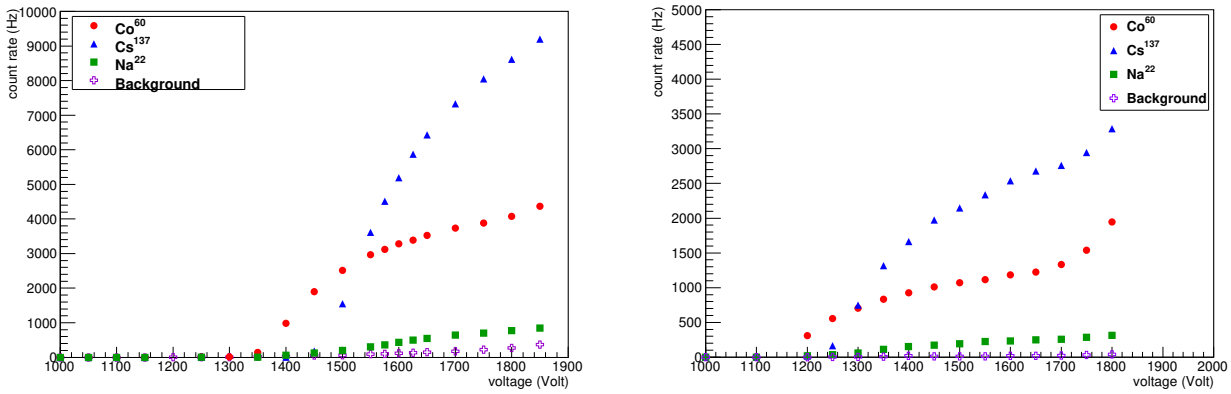

Figure 4.8: Calibration of PMT : Sc-01 (left) and Sc-02 (right)

4.4.2 Threshold Scan of the Scintillator

The threshold scan has been done for both the scintillator detectors using radioactive sources. The high voltage applied to the PMT have been kept constant at 1700 V for both the detectors. Now the threshold have been set at a value of 25 mV and the count has been recorded for three different radioactive sources e.g. Cs^{137}, Na^{22}, Co^{60}. Next the threshold has been increased in steps of 25 mV till 250 mV and same measurements have been repeated for each such steps. The cosmic ray background count has also been taken for each threshold settings and it is subtracted from the count taken with source. The results are shown in Figure 4.9.

4.4.3 Efficiency of Scintillator Sc-01

To obtain the efficiency of Sc-01, three other plastic scintillators, Sc-02, Sc-03 and Sc-04 (same material) have been used as trigger detector. Sc-01 and Sc-04 are of same dimension (20 cm $\times$ 20 cm), whereas Sc-02 and Sc-03 are of size 10 cm $\times$ 2 cm and 10 cm $\times$ 10 cm respectively. The exact arrangement of the scintillators is shown in Figure 4.10.

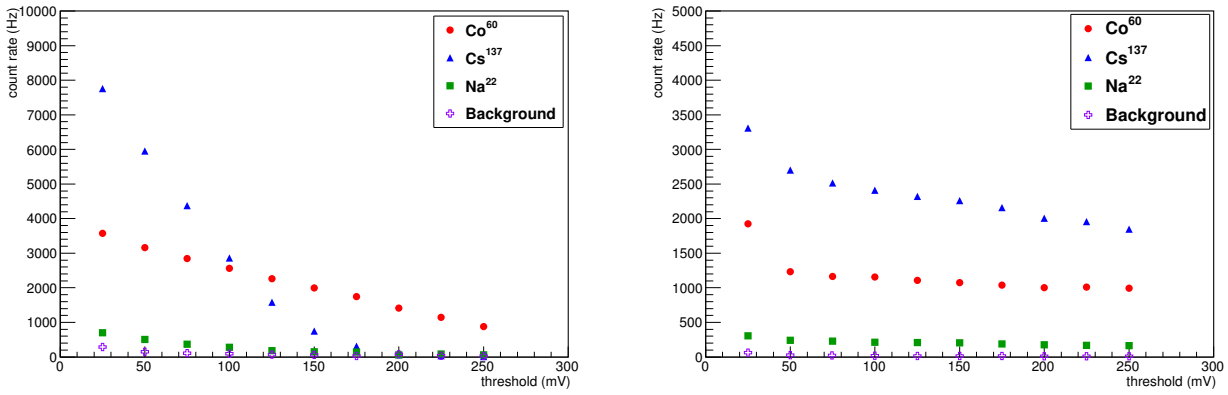

Figure 4.9: Threshold scan of scintillator Sc-01(left) and Sc-02(right)

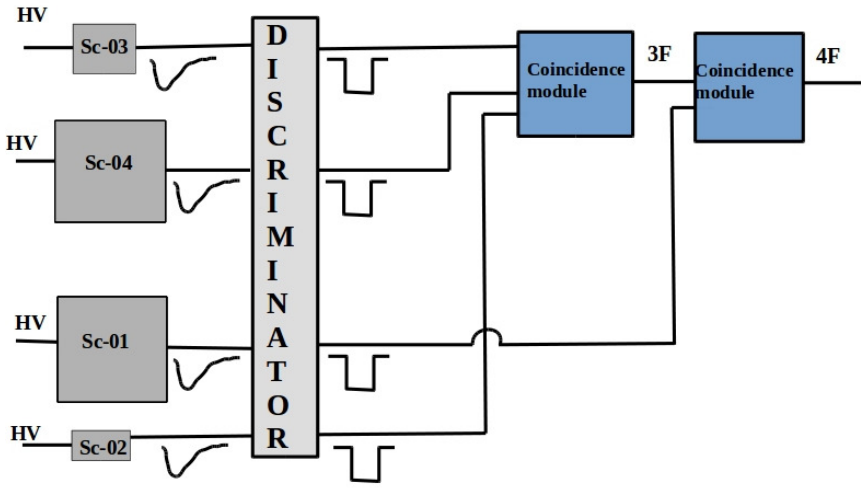

Figure 4.10: Circuit for efficiency measurement of Sc-01

All the PMT's of the trigger scintillator detectors have been kept at HV +1700 V and the voltage of Sc-01 has been increased from 1100 V to 1800 V. The three fold coincidence count obtained from the signals of the scintillators Sc-02, Sc-03 and Sc-04 is taken as the trigger (3F). The coincidence of the trigger and the discriminated signal from Sc-01 is taken and it is the four-fold coincidence (4F). For each voltage settings of Sc-01 the three fold count and four fold count have been measured for a time duration of 30 minutes. A typical three fold coincidence signal obtained from oscilloscope is shown in Figure 4.11. Figure 4.12 shows Sc-01 signal,

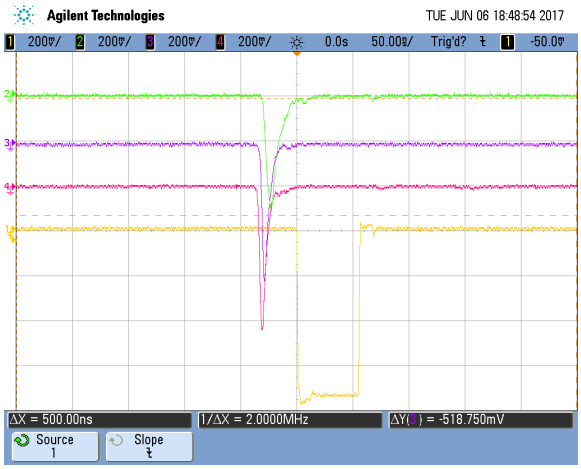

Figure 4.11: Three fold coincidence signal

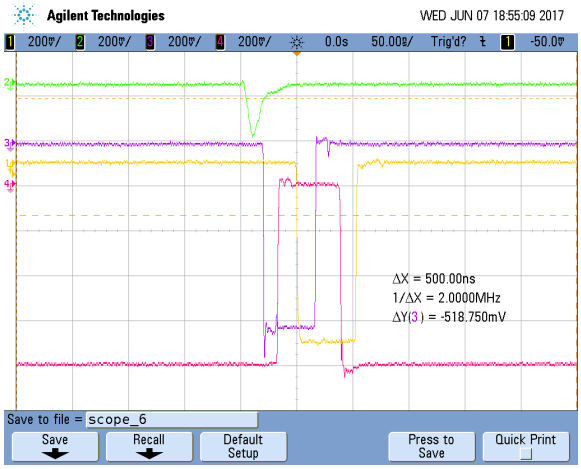

Figure 4.12: Sc-01 signal (green), discriminated signal (purple), three fold trigger (pink) and four fold coincidence (yellow) signal (purple)

discriminated Sc-01 signal, three fold coincidence signal (or trigger) and four fold coincidence signal.

The efficiency is calculated as

$$\%\ Efficiency = \frac{4F}{3F} \times 100\% \tag{4.1}$$

The efficiency as a function of voltage is shown in Figure 4.13. It is found that the efficiency increases with voltage and reaches a plateau above 1400 V.

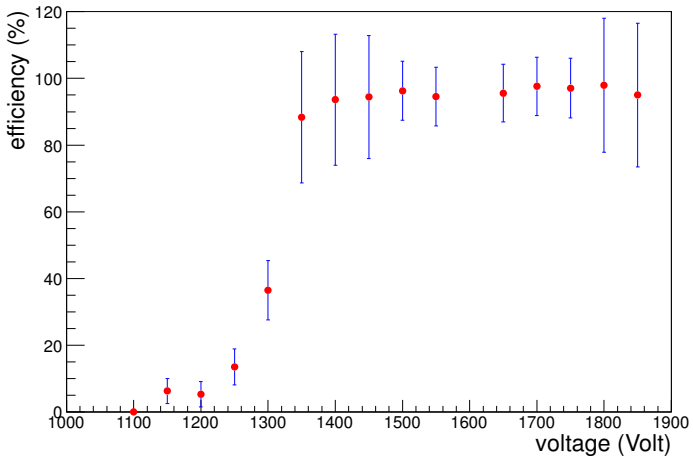

Figure 4.13: Efficiency of scintillator Sc-01

4.4.4 Yield uniformity of paddle scintillator

Yield uniformity have been checked using Fe^{55} source enclosed in a collimator of 4 mm diameter opening. The active area of the scintillator Sc-01 have been divided in 64 imaginary grids each of area 2.5 cm $\times$ 2.5 cm. The Fe^{55} source have been placed at the center of each grid and count have been measured for a time duration of 60 seconds. The results are shown in Figure 4.14. Though the yield is uniform in the central region, there is a variation of 14% in the entire scintillator. The measured yield in the entire scintillator is shown Figure 4.14.

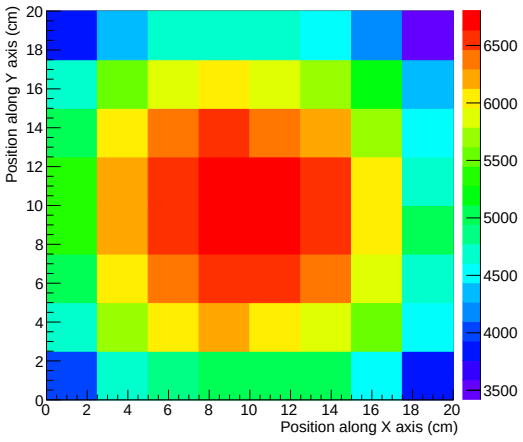

Figure 4.14: Yield uniformity of paddle scintillator

Chapter 5

Measurement of angular variation of cosmic ray flux with scintillator detector

5.1 Introduction

A new and simple technique has been developed using plastic scintillator detectors for the study of angular variation of cosmic ray flux near the sea level.[19]

Cosmic rays are high energy particles that mostly originate from outer space, with some very high energy particles even thought to have extra galactic origin. Primary cosmic rays consist of 90% protons, 9% alpha particles, and of other heavier nuclei. Secondary cosmic rays are created once primary cosmic rays react with gas molecules in the atmosphere. These secondary particles consist mostly of pions and some kaons. Neutral pions(π^0) decay into gamma rays that generate electromagnetic showers (e^+, e^-, γ) which are not very penetrating. Charged pions(π^+, π^-) decay into muons and neutrinos. Neutrinos have very small cross section for interaction and typically pass through the earth without any further interactions.
Cosmic rays lose energy as they travel through matter, mainly through ionization. The Bethe-Bloch equation describes the energy loss of a particle due to ionization.

$$-\frac{dE}{dx} = \frac{4\pi}{m_e c^2}.\frac{nz^2}{\beta^2}.(\frac{e^2}{4\pi\epsilon_O})^2.\{ln(\frac{2m_e c^2\beta^2}{I.(1-\beta^2)}) - \beta^2\} \tag{5.1}$$

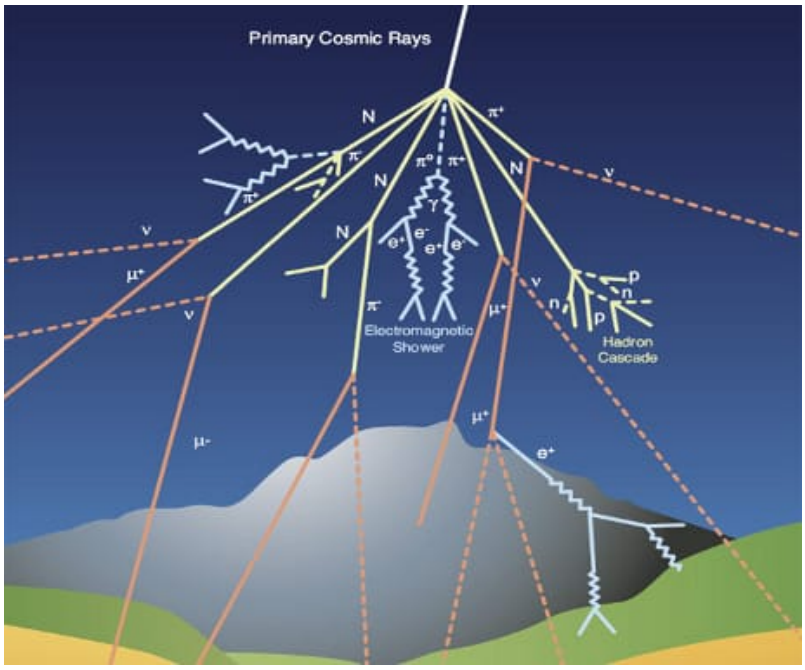

Figure 5.1: Cosmic Rays falling on earth

Radiation loss produced by the deceleration of a charged particle when deflected by another charged particle is a phenomena called Bremsstrahlung. For a given momentum impulse, Bremsstrahlung is inversely proportional to the mass^2 of the radiating particle. The muon is essentially a heavy electron. It has the same spin, and charge but the muon is 200 times heavier than the electron. Muons are unstable; the positive muon (μ^+) decays into a positron and two neutrinos, and the negative muon (μ^-) decays into an electron and two neutrinos. Bremsstrahlung is negligible for muons due to its larger mass but crucial for electrons. This makes the muon a very penetrating particle unlike the electron. The muon has a lifetime of 2.2 μs yet it still makes it down to detectors at the surface of the earth penetrating the atmosphere (480 km thick). This is due to the fact that the muon travels close to the speed of light and so experiences relativistic time dilation, therefore we can detect them.

5.2 Experimental Set-up

In this study the paddle scintillator has been kept fixed in position and the position of the finger detector has been changed. The detectors are placed in a specialized aluminium rack where

both vertical (y axis) and horizontal (x axis) movements are easily possible. The schematic of the experimental set-up is shown in Figure 5.2.

Figure 5.2: Experimental set-up to study angular variation of cosmic ray flux

A bias voltage of 1650 V has been applied to both the detectors. The signals from the scintillator are fed to a leading edge discriminator. Thresholds to the discriminator are set at -50 mV.

The x-axis is chosen to be parallel to the east-west direction. The number of coincidence signals are counted for different angle of incidence of the cosmic rays for a time duration of 60 minutes. The Sc-02 is kept below the Sc-01 along vertical direction. Sc-02 is moved in horizontal plane and coincidence counts are measured at different positions of Sc-02 (along x axis). Thus the incident cosmic ray flux within the solid angle subtended by Sc-01 at Sc-02 for a particular angle of incidence are measured. This measurement is performed for different zenith angles. The expression for solid angle in steradian is calculated using a 2D integration program in ROOT. The coincidence count rate for different zenith angles of cosmic rays has been normalized by the solid angle. The same experiment is repeated with different perpendicular separation between Sc-01 and Sc-02. The singles count for both the scintillators are also measured in each set of readings to check the consistency of data. No remarkable variations in singles count have been observed. The cosmic ray shower rate, measured keeping two scintillators at a separation of

3 m has been found to be $\sim 10^{-5}$ per second per unit area and has been subtracted from all data points.

In this report a detailed description of the angular variation of cosmic rays is presented along with voltage scan and threshold scan of the photomultiplier tube. A study of the uniformity of the paddle scintillator is also performed.

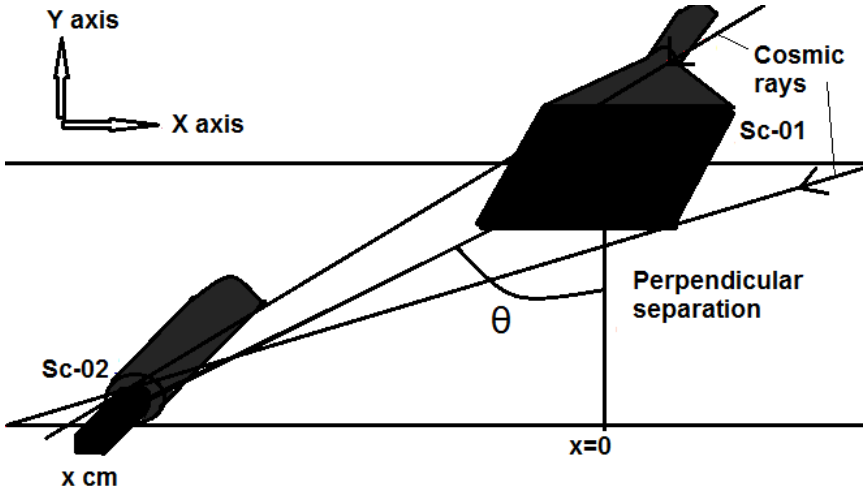

Figure 5.3: Schematic arrangement of Sc-01 and Sc-02 to study angular variation of cosmic rays.

5.3 Angular Variation of cosmic rays

To measure the angular variation of the cosmic ray flux, the detectors have been moved as described in Sec 5.2. Firstly the detector Sc-02 has been kept on the lower rack just below the Sc-01 scintillator as shown in Figure 5.3 This position of Sc-02 has been marked as origin of the x axis. Coincidence count rates of Sc-01 and Sc-02 have been measured for this arrangement. This reading corresponds to the cosmic rays that are vertically incident on our setup. Sc-02 has been moved 5 cm along positive x-axis and measurements were repeated. This reading corresponds to the cosmic rays incident at a zenith angle given by $\theta = \tan^{-1}(5/y)$ in degrees, where y is the perpendicular separation of Sc-01 and Sc-02. Measurements have been repeated by moving Sc-02 in a step of 5 cm along x axis. Thus coincidence count rates for different

zenith angle has been measured. The same process have been done by moving Sc-02 along negative x axis. The average of the coincidence counts of both positive and negative x-axis have been taken. A second method to measure the angular variation of cosmic rays had also been used. In this method, the position of Sc-01 was fixed, and Sc-02 was moved vertically along y axis keeping the separation of Sc-01 and Sc-02 along x axis same. First Sc-01 and Sc-02 were kept on the same plane (xz plane) and coincidence counts of Sc-01 and Sc-02 was measured. This count corresponds to the count for cosmic rays traveling horizontally. Then, the scintillator Sc-02 is moved downwards along y axis and coincidence counts are measured at various such y positions. The cosmic ray showers incident on our set up and also the chance coincidence counts were found to be negligible. The solid angle $\Omega(\theta)$ subtended by Sc-01 at Sc-02 has also been calculated for each of such cosmic ray incidence angles and the coincidence counts were normalized by $\Omega(\theta)$. The calculation of the solid angle is included in Appendix A. Counts have been measured for a time duration of 60 minutes for each setting. The coincidence count rates per unit solid angle per unit area as a function of the zenith angle is shown in Figure 5.4. It is seen from Figure 5.4 that the cosmic ray intensity decreases from $\sim\ 7 \times 10^{-3}$ to $3 \times 10^{-3}\ s^{-1}cm^{-2}sr^{-1}$ corresponding to a zenith angle of 0^o to 70^o respectively.

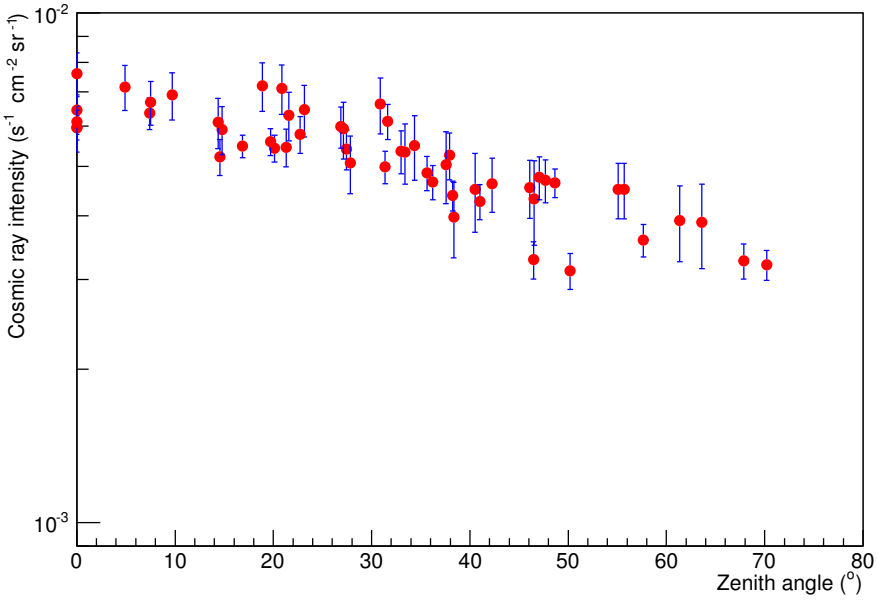

Figure 5.4: Variation of cosmic rays intensity with the zenith angle

5.4 Summary and outlook

One plastic scintillator paddle and one finger detector are fabricated. The count rates are measured for both the detectors with cosmic rays, Co^{60} , Cs^{137} and Na^{22} sources. The yield uniformity of the paddle detector has been carried out. The angular variation of cosmic ray flux is measured with the coincidence technique and it is found that the cosmic ray flux decreases with increasing zenith angle.

The same measurement with scintillators of same dimension and taking coincidence with more than two scintillators are in future plan. The study of east-west asymmetry of cosmic muons will also be done.

Chapter 6

Summary and Discussions

A study of basic characteristics of the straw tube detector have been carried out with premixed gas of Ar+CO_2 70:30 using conventional NIM electronics. In this study count rate, ion charge per particle or the effective gain, signal attenuation and uniformity of performance are measured systematically. The count rates are measured with a strong Fe^{55} X-ray source. The gain and energy resolution are measured from the Fe^{55} spectra varying the voltage. The gain increases exponentially and energy resolution decreases with voltage.

The study of variation of effective gain and energy resolution on the rate will be performed from the energy spectrum of Fe^{55} X-ray source using MCA at different gas mixtures and different flow rates for the straw tube detector. Use of the straw tube detector in CBM MuCh is under investigation.

Several plastic scintillator modules have been fabricated and tested with cosmic ray muons and different radioactive sources at Detector Lab in CAPSS, Bose Institute. Characteristics of two such plastic scintillator detectors, one paddle (named Sc-01) of dimension 20 cm $\times$ 20 cm and one finger scintillator (named Sc-02) of dimension 10 cm $\times$ 2 cm, each of thickness 1 cm, have been studied systematically. A new and simple technique, using the scintillators has been developed to measure the variation of cosmic ray intensity with the zenith angle at the sea level. All the counts of triggered cosmic rays are taken during the daytime. A detailed description of the angular variation of cosmic rays have been made along with voltage scan and threshold scan of the photomultiplier tube. Singles count rate of the scintillators were measured everyday. No such remarkable difference has been noticed. A study of the uniformity of the

paddle scintillator is also performed with two radioactive sources. Cosmic shower rate has also been measured using two fold coincidence technique and is found to be negligible. However, the same measurements will be done using three fold coincidence technique with scintillators of same or nearly same dimensions, so as to get a better physical result. Future plans include the study of east-west asymmetry of cosmic muons.

In this report two different types of detectors and their characteristics have been discussed. It is important to note that not only the working principle of the detectors are different but also the area of applications and limitations are different. Plastic scintillators are basically used as trigger detector in high-energy physics experiments and for detection of cosmic rays, whereas the straw tube detectors are used for particle tracking with low material budget.

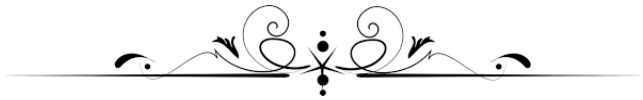

Appendix A

Determination of solid angle subtended by a square scintillator Sc-01 at the centre of a small rectangular scintillator Sc-02

A solid angle is a 2D angle in 3D space that an object subtends at a point. It is defined mathematically as:

$$d\Omega = \frac{ds.cos\theta}{r^2} \tag{A.1}$$

where ds is an elementary area of the object, and $\vec{r}$ is the position vector of the elementary area ds. cos θ is multiplied because the area projected to the point is the only concern.

Let us consider a thin square plate (scintillator) Sc-01 of dimension L $\times$ L as shown in Figure A.1. First, we will find out the solid angle subtended by this plate at a small thin square plate of area b $\times$ b. Then, we will generalise our result (taking some approximation) to an expression which will give us the solid angle subtended by a square plate at a rectangular plate. In principle we can divide our scintillator Sc-02 into five imaginary squares. For instance we calculate the solid angle subtended by Sc-01 at the centre of such an imaginary square plate.

Now, consider an elementary area

$$ds = dx.dy \tag{A.2}$$

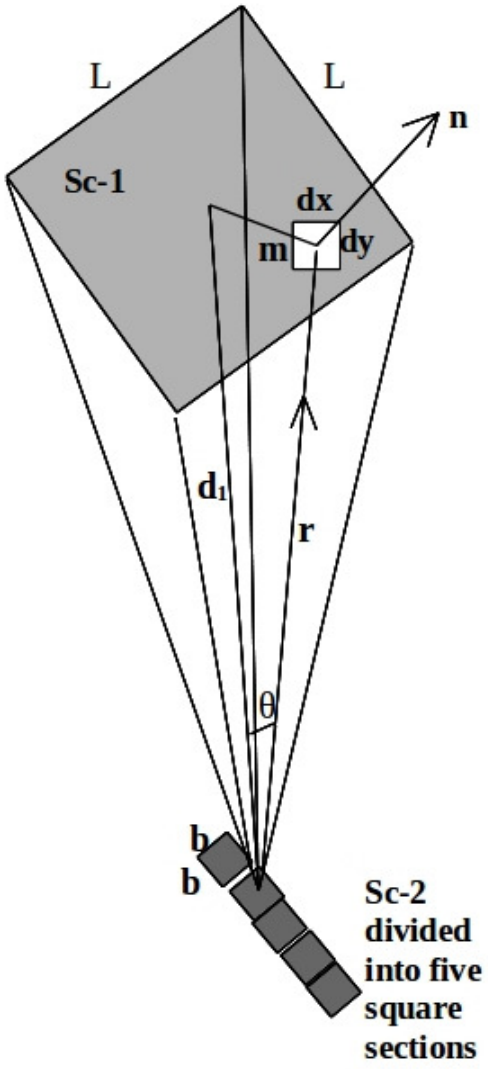

Figure A.1: Schematic diagram showing the solid angle subtended by Sc-01 at a point

whose position vector is $\vec{r}$, (taking the centre of the small square as the origin). $\hat{n}$ is normal to the surface ds. The position vector of the elementary area with respect to the centre of Sc-01 is $\hat{m}$ given by:

$$m^2 = x^2 + y^2 \tag{A.3}$$

where (x,y) is the coordinate of the centre of the elementary area.

Let d_1 be the distance between Sc-01 and Sc-02. From the geometry and Pythagoras theorem,

we have

$$r^2 = d_1^2 + m^2 \tag{A.4}$$

and

$$cos\theta = \frac{d_1}{r} \tag{A.5}$$

So, from the definition of solid angle, dΩ subtended by an elementary area of Sc-01 at point lying on the axis passing through its centre at a distance d_1 is given by:

$$\begin{aligned} d\Omega &= \frac{ds.cos\theta}{r^2} \\ &= \frac{dx.dycos\theta}{r^2} \\ &= \frac{d_1.dx.dy}{\left(d_1^2 + x^2 + y^2\right)^{3/2}} \end{aligned} \tag{A.6}$$

$$\tag{A.7}$$

So, the solid angle subtended by Sc-01 at the centre of the small square is the double integration of $d\Omega$

$$\begin{aligned} \Omega &= \int\int d\Omega \\ \Omega &= \int_{y=-l/2}^{+l/2}\int_{x=-l/2}^{+l/2} \frac{d_1.dx.dy}{\left(d_1^2 + x^2 + y^2\right)^{3/2}} \end{aligned} \tag{A.8}$$

Since the actual solid angle to be found out in the physical situation is not the solid angle subtended by Sc-01 at a point, instead we need to find out the solid angle that Sc-01 subtends at Sc-02. Assuming that Sc-02 is very small compared to the size of Sc-01, we divide the Sc-02 into five equal squares, find out the solid angle subtended at each square and then multiply the number by five to get the approximated solid angle we require. To find out the solid angle subtended at each small square, we adopt a simpler method. Instead of integrating Ω over the surface of the small square, we modify the distance d_1 at which we were calculating the solid angle. Consider figure A.2

We can clearly see that the solid angle subtended by Sc-01 at the square is same as the solid angle subtended at a farther point at a distance d from the centre of Sc-01. Hence, from the

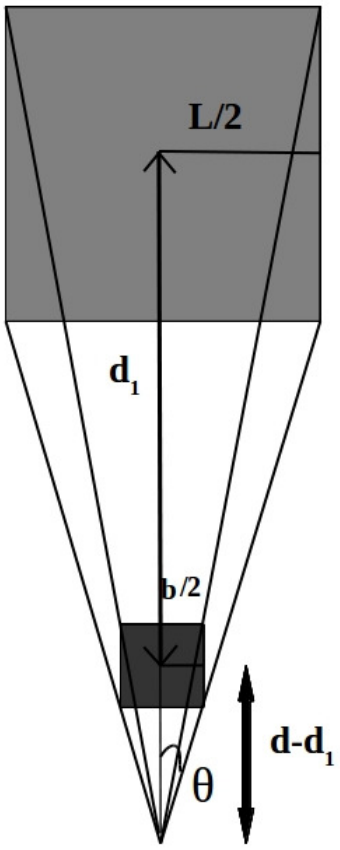

Figure A.2: Geometry of Sc-01 and an imaginary small square

geometry, we can find out the value of d and perform the same integration replacing d_1 by d.

$$\begin{aligned} tan\theta &= \frac{l}{2d} \\ &= \frac{b}{2(d-d_1)} \end{aligned} \tag{A.9}$$

Therefore,

$$\begin{aligned} l(d-d_1) &= bd \\ d &= \frac{ld_1}{(l-b)} \end{aligned} \tag{A.10}$$

Therefore the final expression for Solid angle subtended by Sc-01 at Sc-02 is

$$\Omega = 5 \times \int_{y=-l/2}^{+l/2} \int_{x=-l/2}^{+l/2} \frac{d.dx.dy}{(d^2+x^2+y^2)^{3/2}} \tag{A.11}$$

where the value of d is obtained from equation A.10. Typically, the value of solid angle subtended by a 20 cm $\times$ 20 cm plastic scintillator Sc-01 at 10 cm $\times$ 2 cm finger scintillator Sc-02,

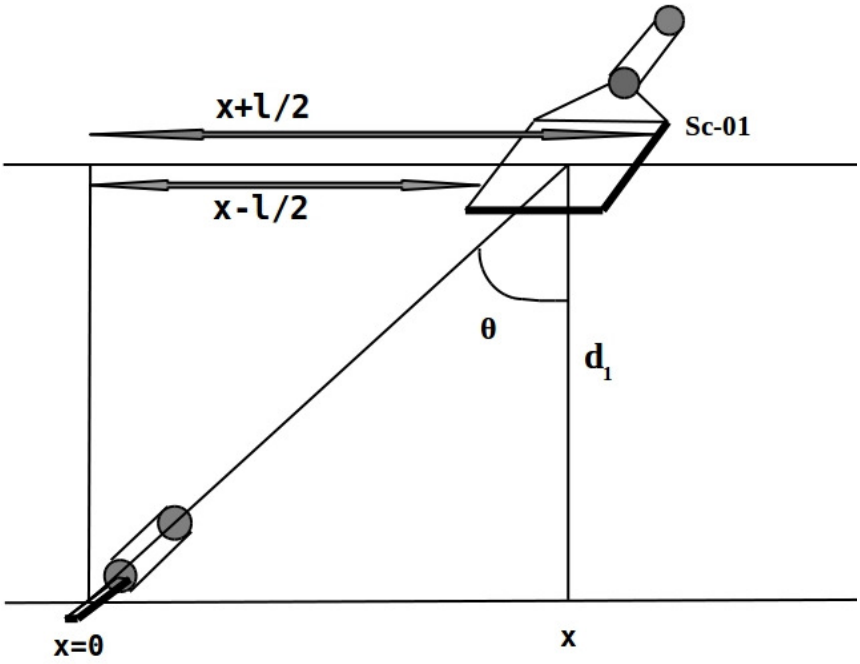

Figure A.3: Arrangement of Sc-01 and Sc-02 detecting cosmic rays incident at a zenith angle θ

is 5×0.211 sr, when Sc-01 and Sc-02 are at perpendicular separation of 38.5 cm. This value has been calculated numerically with a precision of 0.0001. Now, in our experiment described in Chapter 5 Section 5.3, we had to calculate the solid angle subtended by Sc-01 at Sc-02 and normalise the cosmic ray intensity by it. To study the zenith angle dependence of cosmic rays the Scintillator Sc-02 kept at a distance d_1 from Sc-01 was shifted along x axis to take measurement for a particular zenith angle θ. Now this reading should be normalised by the solid angle $\Omega = \Omega(\theta)$ which is different from $\Omega(0)$. So, it is necessary to calculate $\Omega(\theta)$. Again, this can be simply done. Figure A.3 shows the arrangement of Sc-01 and Sc-02 with x=0 denoting the position of Sc-02.

The expression for solid angle obtained in equation A.11 can be modified to obtain an expression for $\Omega(\theta)$. By changing the limits of integration of the variable x which was $\int_{x=-l/2}^{+l/2}$ to $\int_{x'=x-l/2}^{x+l/2}$, where x' is the new variable, we have obtained the final expression for $\Omega(\theta)$ as:

$$\Omega(\theta) = 5 \times \int_{y=-l/2}^{+l/2} \int_{x'=x-l/2}^{x+l/2} \frac{d}{\left(d^2 + x^2 + y^2\right)^{3/2}} dx'dy \tag{A.12}$$

There is no change in position of Sc-02 along y axis, so the limits of y need not be changed. Now, having the expression A.12 in hand, we can just perform the integration using a 2D integration program in ROOT and calculate $\Omega(\theta)$ at required values of θ.

Bibliography

[1] P. J. Ouseph: Introduction to Nuclear Radiation Detectors, (Springer-Verlag Berlin Heidelberg GmbH)

[2] M. Aglietta et al., *The EAS-TOP array at Gran Sasso: results of the electromagnetic detector*, *Nucl. Phys B* **16** (1990), 493.

[3] M. Aglietta et al., *Detection of the UHE Burst from the Crab Nebula on February 23, 1989, from the EAS-TOP Array*, *Europhysics Letters 1* **15** (1991) 81.

[4] KASCADE Collaboration, *Electron, muon, and hadron lateral distributions measured in air showers by the KASCADE experiment*, *Astroparticle Physics* **14** (2001) 245.

[5] W.D. Apel et al., *The KASCADE-Grande experiment*, *Nucle. Instr. Meth. A* **620** (2010) 202.

[6] S.K. Gupta et al., *The current status of the GRAPES-3 extensive air shower experiment*, *Nuclear Physics B - Proceedings Supplements* **196** (2009) 153M.

[7] S.K. Gupta et al., *GRAPES-3 A high-density air shower array for studies on the structure in the cosmic-ray energy spectrum near the knee*, *Nuclear Instruments and Methods in Physics Research A* **540** (2005) 311.

[8] http://www.fair-center.eu/for-users/experiments/cbm.html .

[9] http://www.fair-center.eu/ .

[10] C. Adorisio et al., *A non-invasive technique to replace the anode wires into the drift tube chambers of the muon spectrometer of the ATLAS experiment at the LHC proton-proton collider*, *Nuclear Instruments and Methods in Physics Research Section A* **575** (2007) 532.

[11] R.P. Adak et al., *Long-term stability test of a triple GEM detector*, *2016 JINST 11 T10001* doi:10.1088/1748-0221/11/10/T10001.

[12] T. Akesson et al., *Straw tube drift-time properties and electronics parameters for the ATLAS TRT detector*, *Nuclear Instruments and Methods in Physics Research Section A* **449** (2000) 446.

[13] T. ρAkesson et al., *Study of straw proportional tubes for a transition radiation detector/tracker at LHC*, *Nuclear Instruments and Methods in Physics Research Section A* **361** (1995) 440.

[14] PANDA Collaboration, *Technical Design Report for the: PANDA Straw Tube Tracker*, *arXiv:1205.5441.*

[15] R. P. Adak et al., *Study of characteristics of Straw Tube detector for CBM Muon Chamber*, *CBM Progress Report* (2016) 83.

[16] A.N. Dmitrieva et al., arXiv:hep-ex/0611051v1.

[17] Alexander Mishev, arXiv: physics/0602120 v.2 .

[18] S. Cecchini and M. Spurio, arXiv:1208.1171v1.

[19] Mehmet Bektasoglu and Halil Arslan, Pramana - Journal of Physics, Vol. 80, No. 5, May 2013, pp 837 - 846.

[20] ROOT, A Data Analysis Framework, CERN, website: <http://www.root.cern.ch>.

[21] Glenn F. Knoll: Radiation Detection and Measurement, (Third Edition, John Wiley and Sons, Inc.).

[22] William R. Leo: Techniques for Nuclear and Particle Physics Experiments,A How-to Approach, (Second Revised Edition, Springer-Verlag Berlin Heidelberg GmbH)

Outcome of the project

- **R&D on Straw Tube detector for CBM Muon Chamber.**
  Authors: R. P. Adak, S. Biswas, S. Chattopadhyay, S. Das, D. Ghosal, P. Ghosal, A. Mondal, D. Nag, **S. Roy**, and J. Saini
  Published in **Proceedings of the DAE-BRNS Symposium on Nuclear Physics. Volume 61, (2016), 996-997.**

- **Study of some aspects of straw tube detectors for CBM-MuCh.**
  Authors: **S. Roy**, R. P. Adak, S. Biswas, S. Chatttopadhyay, S. Das, D. Ghosal, S. K. Ghosh, A. Mondal, D. Nag, D. Paul, S. K. Prasad, S. Raha, and J. Saini
  Oral presentation in **INSTR17: International Conference "Instrumentation for Colliding Beam Physics", Budker Institute of Nuclear Physics, and Novosibirsk State University, Novosibirsk, Russia.**

- **Some aspects of characterization of GEM detector.**
  Authors: D. Nag, D. Paul, **S. Roy**, S. Biswas, S. Das, S. K. Ghosh, S. K. Prasad, S. Raha
  Presented in **Advanced Detectors for Nuclear, High Energy and Astroparticle Physics.**
  Accepted in **Springer Proceedings in Physics.**

- **Measurement of angular variation of cosmic rays with plastic scintillator detector.**
  Authors: **S. Roy**, R. P. Adak, R. Biswas, D. Nag, D. Paul, S. Rudra, S. Biswas, S. Das
  Presented in **Advanced Detectors for Nuclear, High Energy and Astroparticle Physics.**